Chapter 1

Comparison of the standard and dressed-picture master equations for the quantum Rabi model in the ultrastrong coupling regime

arXiv:2604.08852v2 [quant-ph] 21 Jul 2026

Alexandre P. Costa[1], Hebert S. Rego de Oliveira[1] and Alexandre Dodonov[1,2,a]

[1] Institute of Physics, University of Brasília, 70910-900, Brasília, DF, Brazil
[2] International Center of Physics, Institute of Physics, University of Brasília, 70910-900, Brasília, DF, Brazil
[a] adodonov@unb.br

1.1 Abstract

The goal of this chapter is to investigate the effects of relaxation and dephasing on the quantum Rabi model in the ultrastrong coupling regime, and to provide explicit formulas that enable students and researchers to implement and numerically solve the resulting nonunitary dynamics from first principles. The quantum Rabi model constitutes the most fundamental description of light–matter interaction, describing a single two-level system coupled to a single mode of a quantized cavity field. The ultrastrong coupling regime is typically defined by coupling strengths satisfying $g \gtrsim 0.1\,\omega$, where ω denotes the cavity-mode frequency. In this regime, the standard master equation of Quantum Optics—commonly referred to as the Gorini–Kossakowski–Sudarshan–Lindblad (GKSL)

[1] Chapter 5 of the book "Modern Topics in Mathematical, Quantum and Statistical Physics: Proceedings of the 2025 CIF-UnB conferences". DOI: 10.29327/5868499. ISBN: 978-65-5563-767-0.

master equation—is expected to become inaccurate. The underlying reason is that strong light–matter interaction hybridizes the bare atom and field states, so that dissipation can no longer be consistently described in the uncoupled basis. A more consistent treatment must therefore incorporate this hybridization directly into the derivation of the dissipative terms. One such approach is the dressed-picture Markovian master equation derived by Beaudoin, Gambetta, and Blais, in which the qubit–field interaction is explicitly included when constructing the system–bath coupling operators. In this chapter, we numerically solve both the standard GKSL master equation and the dressed-picture master equation (DME) for various initial field states, including coherent states, odd Schrödinger cat states, squeezed vacuum states, squeezed coherent states, and thermal states. The coupling strength is varied in the range $0.05\,\omega$ to $0.8\,\omega$. We also examine photon generation from the vacuum induced by external time-dependent modulation of the qubit parameters, as well as multiphoton Rabi oscillations for an initially excited qubit. Two different reservoir spectral densities are considered: white noise and Ohmic noise. The differences between the two master-equation approaches are illustrated through numerical results for several physical observables, including the qubit excited-state population, the mean photon number, the Mandel Q-factor, the negativity (used as a measure of entanglement), the subsystem purities, and the photon-number probability distribution at selected times. As expected, for many of these quantities the predictions of the standard GKSL master equation differ substantially from those of the dressed-picture master equation. However, in certain parameter regimes and for specific observables, the discrepancies remain comparatively small.

1.2 Introduction

Open quantum systems constitutes the field of Quantum Physics devoted to understanding how a system of interest interacts with its surrounding environment and how this interaction leads to dissipation, decoherence, and noise. Although the combined system+environment composite evolves unitarily according to the Schrödinger equation, the reduced dynamics of the system alone is generally nonunitary and must be described using density operators and dynamical maps, often in the form of master equations (MEs). Central topics in this area include the derivation and the evaluation of the validity of Markovian and non-Markovian master equations for different physical implementations and regimes of parameters [1–7].

The study of open quantum systems in the ultrastrong coupling (USC) regime has attracted considerable attention over the past decade, particularly due to the breakdown of standard quantum-optical approaches when the light–matter coupling strength becomes a significant fraction of the cavity frequency [8–11]. In the USC regime, defined by $g \gtrsim 0.1\omega$, the rotating-wave approximation fails and the eigenstates of the system become strongly hybridized. As a consequence, dissipative treatments based on the standard Gorini–Kossakowski–Sudarshan–Lindblad (GKSL) master equation derived in the bare basis may lead to unphysical predictions [12–14].

A seminal contribution in this context is the work of *Beaudoin, Gambetta, and Blais* [14], who derived a Markovian master equation in the dressed basis (DME, standing for for "dressed master equation") of the quantum Rabi Hamiltonian [15–19]. By incorporating the light–matter interaction directly into the derivation of the dissipative terms, they demonstrated that the standard GKSL master equation can incorrectly predict spurious

excitations and inaccurate steady states in the USC regime. Although significantly more realistic than the GKSL ME (and harder to solve, both analytically and numerically), this equation relied on the secular (rotating-wave) approximation, so that its validity is compromised in the dispersive regime and at relatively high photon numbers in cavity and circuit QED. Shortly afterwards, [20] showed how to derive a dressed master equation valid in the dispersive regime; [21] provided a systematic microscopic derivation of the dressed master equation and the quantum Langevin equation; [22] derived a generalized DME without performing the secular and low-photon-number approximations; and [23] presented a gauge-invariant dressed master equation. Recently, alternative master equations valid in the USC regime were presented in [24, 25]. It is worth noting that the numerically "exact" dynamics of a reduced system under nonperturbative and non-Markovian system–bath interactions can be obtained via computationally expensive hierarchical equations of motion (HEOM), as described in the review [26].

Although dressed-state master equations are, in principle, more accurate than the standard GKSL equation in the ultrastrong coupling regime, they present a significant practical drawback: analytical solutions are generally out of reach, and numerical implementations require substantial computational resources and algorithmic care. In particular, the derivation and implementation of the dressed master equation involve diagonalization of the interacting Hamiltonian and the evaluation of transition rates in the dressed basis, which considerably increases numerical complexity. Consequently, these equations are not immediately accessible to researchers entering the field. Even the numerical solution of the standard GKSL master equation for Hilbert spaces involving on the order of 100 photons already demands nontrivial computational time and memory.

For this reason, in this chapter we provide a step-by-step tutorial on how to numerically solve both the GKSL master equation and the dressed master equation of Beaudoin, Gambetta, and Blais. We then illustrate the typical dissipative dynamics for a variety of initial states, coupling strengths, and qubit–field detunings. Our numerical results show that, depending on the parameter regime and the observable considered, the predictions of the two master equations may either agree reasonably well or differ dramatically. We therefore hope that this chapter will serve as a practical guide for students and researchers performing their own numerical studies, while our examples help delineate the regimes in which the simpler GKSL master equation provides an acceptable approximation within a given accuracy threshold.

This chapter is organized as follows. The GKSL ME is described in Section 1.3 and DME — in Section 1.4. Then we illustrate the typical behavior for the coherent (Section 1.5), odd Schrödinger cat (Section 1.6), squeezed coherent (1.7), squeezed vacuum (1.8), and thermal (Section 1.9) states. Section 1.10 shows the results for the multiphoton Rabi oscillations for the initial excited state of the qubit. In Section 1.11 we study the photon generation from vacuum via external modulation of the qubit transition frequency combined with the preparation of the cavity field state via post-selection protocols, showing that the generated cavity field state display metrological power. Finally, Section 1.12 contains the summary of this work.

1.3 GKSL master equation

A general master equation for the density operator ρ can be written as

$$\frac{d\rho}{dt} = -i\,[H,\rho] + L\rho \tag{1.1}$$

where H is the system Hamiltonian, $[,]$ is the commutator and L is the Liouvillian superoperator that depends on the particular master equation and whose form can be quite complicated. The Gorini–Kossakowski–Sudarshan–Lindblad (GKSL) master equation, also known as the standard master equation of Quantum Optics and derived in almost every introductory textbook on the subject [1–5], reads

$$L_{GKSL} = \kappa_0\,(\bar{n}_\omega + 1)\,D\,[a] + \kappa_0\bar{n}_\omega D\left[a^\dagger\right] + \gamma_0\,(\bar{n}_\Omega + 1)\,D\,[\sigma_-] + \gamma_0\bar{n}_\Omega D\,[\sigma_+] + \frac{\gamma_\phi}{2}D\,[\sigma_z] \tag{1.2}$$

where κ_0 is the cavity damping (relaxation) rate, γ_0 is the qubit damping rate, γ_ϕ is the qubit pure dephasing rate, ω is the cavity frequency, Ω is the qubit transition frequency and $\bar{n}_\nu = \left[e^{\hbar\nu/k_BT} - 1\right]^{-1}$ is the average thermal photon number for the frequency ν, with T being the reservoir's temperature and k_B the Boltzman constant.. Here a is the cavity field annihilator operator, $a^\dagger$ is the creation operator, $\sigma_- = |g\rangle\langle e|$ is the lowering Pauli operator, $\sigma_+ = |e\rangle\langle g|$ is the raising Pauli operator and $\sigma_z = |e\rangle\langle e| - |g\rangle\langle g|$ is the pauli z-matrix, where $|g\rangle$ and $|e\rangle$ denote the qubit ground and excited states, respectively. The Lindblad dissipator is a superoperator defined as

$$D\,[O]\,\rho = O\rho O^\dagger - \frac{1}{2}\left(O^\dagger O\rho + \rho O^\dagger O\right)\,. \tag{1.3}$$

To solve numerically this master equation for the Rabi Hamiltonian (we set $\hbar = 1$)

$$H = \omega n + \Omega|e\rangle\langle e| + gX\sigma_x\ , \tag{1.4}$$

where $n = a^\dagger a$ is the photon number operator and

$$X = a + a^\dagger\ ,\ \sigma_x = \sigma_+ + \sigma_-\ . \tag{1.5}$$

We expand the density operator in the complete orthonormal basis $\{|g, f_n\rangle, |e, f_n\rangle\}$ as

$$\begin{aligned}\rho \;=\; & \sum_{n,m=1}^{Q_1+1} [A_{nm}|g, f_{n-1}\rangle\langle g, f_{m-1}| + B_{nm}|e, f_{n-1}\rangle\langle e, f_{m-1}| \\ & + C_{nm}|g, f_{n-1}\rangle\langle e, f_{m-1}| + C^*_{mn}|e, f_{n-1}\rangle\langle g, f_{m-1}|]\ ,\end{aligned} \tag{1.6}$$

where $|f_m\rangle$ denotes the m-th Fock state of the field, $n|f_m\rangle = m|f_m\rangle$. For numerical calculations, we need to truncate the Hilbert space at Q_1 photons, assuming that the probability of $m > Q_1$ photons is identically zero (in the actual case, it should be smaller than some threshold value ε, say $\varepsilon \lesssim 10^{-8}$ for all times). The expansion (1.6) permits one to calculate the average value of any operator O as $\langle O\rangle = \mathrm{Tr}\,[\rho O]$. In particular, the average values of operators belonging only to the qubit or to the cavity field can be easily evaluated using the reduced density matrices $\rho_q = \mathrm{Tr}_c\,(\rho)$ or $\rho_c = \mathrm{Tr}_q\,(\rho)$, respectively, where

$$\rho_q = A|g\rangle\langle g| + B|e\rangle\langle e| + C|g\rangle\langle e| + C^*|e\rangle\langle g| \tag{1.7}$$

$$\rho_c = \sum_{N,M=1}^{Q_1+1} D_{NM} |f_{N-1}\rangle\langle f_{M-1}|$$

and

$$A = \sum_{N=1}^{Q_1+1} A_{NN} \ , \ B = \sum_{N=1}^{Q_1+1} B_{NN} \ , \ C = \sum_{N=1}^{Q_1+1} C_{NN} \ , \ D_{NM} \equiv A_{NM} + B_{NM} \ . \tag{1.8}$$

The purities of the qubit and the cavity field are, respectively,

$$\Pi_q = \mathrm{Tr}\, \rho_q^2 = A^2 + B^2 + 2\,|C|^2 \tag{1.9}$$

$$\Pi_c = \mathrm{Tr}\, \rho_c^2 = \sum_{N,M=1}^{Q_1+1} |D_{NM}|^2 \ . \tag{1.10}$$

The negativity [27], whose nonzero values attest entanglement for any bipartite system, is defined as

$$\mathcal{N}(\rho) = \left| \sum_{\lambda_i<0} \lambda_i \right| \ , \tag{1.11}$$

where λ_i are the eigenvalues of the partial transpose of the total system density operator ρ with respect to any subsystem, denoted as ρ^T. In our case, writing

$$\rho = \sum_{n,m=1}^{Q_1+1} \sum_{i,j=1(g)}^{2(e)} \varrho_{i,n;j,m} |i, f_{n-1}\rangle\langle j, f_{m-1}| \ , \tag{1.12}$$

where $|i=1\rangle \equiv |g\rangle$ and $|i=2\rangle \equiv |e\rangle$, the matrix elements of the original and partially transposed density operator are

$$\langle i, f_{n-1}|\rho|j, f_{m-1}\rangle = \varrho_{i,n;j,m} \ , \ \langle i, f_{n-1}|\rho^T|j, f_{m-1}\rangle = \varrho_{j,n;i,m} \ . \tag{1.13}$$

By diagonalyzing the matrix ρ^T, the negativity can be easily found.

From the hermiticity condition $\rho = \rho^\dagger$ we can eliminate the redundant elements by defining for $n > m$

$$\mathrm{Re}\,(A_{nm}) = \mathrm{Re}\,(A_{mn}) \,, \ \mathrm{Im}\,(A_{nm}) = -\,\mathrm{Im}\,(A_{mn}) \,, \ \mathrm{Im}\,(A_{nn}) = 0 \tag{1.14}$$

and similar relations hold for B_{nm}. Then, for $1 \le p \le Q_1 + 1$ and $p \le j \le Q_1 + 1$ we define the $(Q_2+1)^2$-dimensional vector $\mathbf{Y}$ as

$$\mathrm{Re}\,(A_{p,j}) = Y\left[(p-1)\,Q_1 + j - \frac{(p-1)\,(p-2)}{2}\right] \tag{1.15}$$

$$\mathrm{Im}\,(A_{p,j}) = Y\left[F_1 + (p-1)\,Q_1 + j - 1 - \frac{p\,(p-1)}{2}\right] \tag{1.16}$$

$$\mathrm{Re}\,(B_{p,j}) = Y\left[F_2 + (p-1)\,Q_1 + j - \frac{(p-1)\,(p-2)}{2}\right] \tag{1.17}$$

$$\mathrm{Im}\,(B_{p,j}) = Y\left[F_3 + (p-1)\,Q_1 + j - 1 - \frac{p\,(p-1)}{2}\right] \tag{1.18}$$

$$\mathrm{Re}\,(C_{p,j}) = Y\left[F_4 + (p-1)\,(Q_1+1) + j\right] \tag{1.19}$$

$$\mathrm{Im}\,(C_{p,j}) = Y\left[F_5 + (p-1)\,(Q_1+1) + j\right] \ , \tag{1.20}$$

where $Q_2 \equiv 2Q_1 + 1$ and

$$F_1 = \frac{(Q_1+1)(Q_1+2)}{2} \ , \ F_2 = (Q_1+1)^2 \ , \ F_3 = (Q_1+1)^2 + \frac{(Q_1+1)(Q_1+2)}{2} \quad (1.21)$$

$$F_4 = 2(Q_1+1)^2 \ , \ F_5 = 3(Q_1+1)^2 \ . \quad (1.22)$$

After minor algebra, for the zero absolute temperature one obtains the system of coupled ordinary differential equations for the coefficients of the density operator

$$\begin{aligned} \dot{A}_{NM} &= -i\omega(N-M)A_{NM} \\ &\quad -ig\left(\sqrt{N}C^*_{M,N+1} + \sqrt{N-1}C^*_{M,N-1} - \sqrt{M-1}C_{N,M-1} - \sqrt{M}C_{N,M+1}\right) \\ &\quad +\kappa_0\sqrt{NM}A_{N+1,M+1} - \frac{\kappa_0}{2}(N+M-2)A_{NM} + \gamma_0 B_{NM} \end{aligned} \quad (1.23)$$

$$\begin{aligned} \dot{B}_{NM} &= -i\omega(N-M)B_{NM} \\ &\quad -ig\left(\sqrt{N}C_{N+1,M} + \sqrt{N-1}C_{N-1,M} - \sqrt{M-1}C^*_{M-1,N} - \sqrt{M}C^*_{M+1,N}\right) \\ &\quad +\kappa_0\sqrt{NM}B_{N+1,M+1} - \left[\frac{\kappa_0}{2}(N+M-2) + \gamma_0\right]B_{NM} \end{aligned} \quad (1.24)$$

$$\begin{aligned} \dot{C}_{NM} &= -i\left[\omega(N-M) - \Omega\right]C_{NM} \\ &\quad -ig\left(\sqrt{N}B_{N+1,M} + \sqrt{N-1}B_{N-1,M} - \sqrt{M-1}A_{N,M-1} - \sqrt{M}A_{N,M+1}\right) \\ &\quad +\kappa_0\sqrt{NM}C_{N+1,M+1} - \left[\frac{\kappa_0}{2}(N+M-2) + \frac{\gamma_0}{2} + \gamma_\phi\right]C_{NM} \ . \end{aligned} \quad (1.25)$$

Expressing the coefficients A_{NM}, B_{NM} and C_{NM} as components of the vector $\mathbf{Y}$, one obtains the complete description of the dissipative dynamics by solving the system of $(Q_2+1)^2$ ordinary differential equations (ODE) of the form $\dot{\mathbf{Y}} = \mathbf{M}\mathbf{Y}$, where $\mathbf{M}$ is some time-independent square matrix. In our case, we use the Runge-Kutta-Verner fifth-order and sixth-order method to obtain $\mathbf{Y}(t)$, from which the density operator is recovered via relations (1.6) and (1.15) – (1.20).

1.4 Dressed picture master equation

The dressed master equation (DME) derived in [14] has the following Liouvillian at zero absolute temperature

$$L_{DME}\rho = D\left[\sum_j \Phi_j |j\rangle\langle j|\right]\rho + \sum_{j,k>j}\Gamma^{jk}D\left[|j\rangle\langle k|\right]\rho \ , \quad (1.26)$$

where

$$\Phi_j = \sqrt{\frac{\gamma_\phi(0)}{2}}\sigma_z^{jj} \quad (1.27)$$

$$\Gamma^{jk} = \Gamma^{jk}_\phi + \Gamma^{jk}_\kappa + \Gamma^{jk}_\gamma \quad (1.28)$$

$$\Gamma_{\phi}^{jk}=\frac{\gamma_{\phi}\left(\Delta_{kj}\right)}{2}\left|\sigma_{z}^{jk}\right|^{2}\ ,\ \Gamma_{\kappa}^{jk}=\kappa\left(\Delta_{kj}\right)\left|X^{jk}\right|^{2}\ ,\ \Gamma_{\gamma}^{jk}=\gamma\left(\Delta_{kj}\right)\left|\sigma_{x}^{jk}\right|^{2} \tag{1.29}$$

and the matrix elements of any operator O are defined as $O^{nm}=\langle n|O|m\rangle$. Here, $|n\rangle$ is the eigenstate of H with eigenvalue Λ_n, $\Delta_{kj}=\Lambda_k-\Lambda_j$ is the energy difference and we label the eigenstates in the increasing order of energy (i. e., $\Lambda_{k+1}\geq\Lambda_k$). Althought the equation (1.26) seems complicated, it is still much simpler than the generalized dressed master equation [22, 24, 26] or other approaches with fewer underlying approximations [24, 26].

The manner we chose to solve numerically the DME was to expand the density operator in the dressed-states basis as

$$\rho=\sum_{N=0}^{Q_2}\sum_{M=0}^{Q_2}r_{N,M}|N\rangle\langle M| \tag{1.30}$$

where Q_2+1 is the total number of orthonormal states in the truncated dressed-states basis $\{|0\rangle,\ldots|Q_2+1\rangle\}$. From the hermiticity condition $\rho=\rho^{\dagger}$, which implies $r_{n,m}=r_{m,n}^{*}$, we define the components of $(Q_2+1)^2$-dimensional vector $\mathbf{Y}$ via the relations

$$\begin{aligned}
\mathrm{Re}\left(r_{p,j}\right) &= Y\left(p\cdot Q_2+j+1-p\left(p-1\right)/2\right)\ \text{for}\ p\leq j & (1.31)\\
\mathrm{Im}\left(r_{p,j}\right) &= Y\left(\left(Q_2+1\right)\left(Q_2+2\right)/2+p\cdot Q_2+j-p\left(p+1\right)/2\right)\ \text{for}\ p<j & (1.32)\\
\mathrm{Re}\left(r_{p,j}\right) &= \mathrm{Re}\left(r_{j,p}\right);\ \mathrm{Im}\left(r_{p,p}\right)=0;\ \mathrm{Im}\left(r_{p,j}\right)=-\mathrm{Im}\left(r_{j,p}\right)\ \text{for}\ p>j\ . & (1.33)
\end{aligned}$$

After straightforward calculations, one obtains the system of coupled ODE:

$$\begin{aligned}
\mathrm{Re}\left(\dot{r}_{N,M}\right) &= \left(\Lambda_N-\Lambda_M\right)\mathrm{Im}\left(r_{N,M}\right)-\Theta^{N,M}\,\mathrm{Re}\left(r_{N,M}\right)\\
\mathrm{Im}\left(\dot{r}_{N,M}\right) &= -\left(\Lambda_N-\Lambda_M\right)\mathrm{Re}\left(r_{N,M}\right)-\Theta^{N,M}\,\mathrm{Im}\left(r_{N,M}\right)
\end{aligned}$$

for $1\leq M\leq Q_2$ and $N<M$, and

$$\dot{r}_{N,N}^{r}=\sum_{k=N+1}^{Q_2}\Gamma^{Nk}r_{k,k}^{r}-\Upsilon^{N,N}r_{N,N}^{r}\ ,\ \text{for}\ 0\leq N\leq Q_2\ ,$$

where

$$\Theta^{N,M}=\frac{\gamma_{\phi}\left(0\right)}{4}\left(\sigma_{z}^{NN}-\sigma_{z}^{MM}\right)^{2}+\Upsilon^{N,M} \tag{1.34}$$

$$\Upsilon^{N,M}=\frac{1}{2}\left(\sum_{j=0}^{N-1}\Gamma^{jN}+\sum_{j=0}^{M-1}\Gamma^{jM}\right)\ ,\ \Upsilon^{N,N}=\sum_{j=0}^{N-1}\Gamma^{jN}\,. \tag{1.35}$$

We see that only the diagonal elements have many terms on the right-hand side, which turns the system relatively easy to solve numerically after one determines the dressed states either exactly or numerically.

Here we find the dressed states by diagonalizing the Rabi Hamiltonian in the complete basis $\{|g,f_n\rangle,|e,f_n\rangle\}$. So we write

$$|n\rangle=\sum_{i=1}^{Q_1+1}c_{i,n}|g,f_{i-1}\rangle+\sum_{i=Q_1+2}^{Q_2+1}c_{i,n}|e,f_{i-(Q_1+2)}\rangle\ \text{for}\ 0\leq n\leq Q_2\ , \tag{1.36}$$

where Q_1 is the truncation photon number and $Q_2 = 2Q_1 + 1$. In this basis, the matrix elements read

$$\sigma_z^{nm} = -\sum_{i=1}^{Q_1+1} c_{i,n}^* c_{i,m} + \sum_{i=Q_1+2}^{Q_2+1} c_{i,n}^* c_{i,m} \tag{1.37}$$

$$\sigma_x^{nm} = \sum_{i=1}^{Q_1+1} c_{i,n}^* c_{i+Q_1+1,m} + \sum_{i=Q_1+2}^{Q_2+1} c_{i,n}^* c_{i-Q_1-1,m} \tag{1.38}$$

$$\begin{aligned} X^{nm} &= \sum_{i=1}^{Q_1} \sqrt{i} c_{i,n}^* c_{i+1,m} + \sum_{i=2}^{Q_1+1} \sqrt{i-1} c_{i,n}^* c_{i-1,m} \\ &+ \sum_{i=Q_1+2}^{Q_2} \sqrt{i-Q_1-1} c_{i,n}^* c_{i+1,m} + \sum_{i=Q_1+3}^{Q_2+1} \sqrt{i-Q_1-2} c_{i,n}^* c_{i-1,m} \ , \end{aligned} \tag{1.39}$$

from which all the dissipative rates Γ_κ^{jk} can be found provided the spectral densities of the reservoirs are known. In this work we consider two standard examples of spectral densities (recalling that for the considered zero-temperature regime, the spectral densities are zero for negative frequencies: $\gamma(\Delta_{kj}) = \gamma_\phi(\Delta_{kj}) = \kappa(\Delta_{kj}) = 0$ for $\Delta_{kj} < 0$). For the *white noise* [14], we assume that $\gamma(\Delta_{kj}) = \gamma_0$, $\gamma_\phi(\Delta_{kj}) = \gamma_\phi$ and $\kappa(\Delta_{kj}) = \kappa_0$ for $\Delta_{kj} \geq 0$, where γ_0, γ_ϕ and κ_0 are constant damping rate used in the GKSL ME. For the ohmic noise [22, 28], we assume $\gamma_\phi(\Delta_{kj}) = \gamma_\phi$ for the pure dephasing, while for the relaxation processes we postulate

$$\gamma(\Delta_{kj}) = \gamma_0 \frac{\Delta_{kj}}{\Omega} \exp\left(-\frac{\Delta_{kj}}{\Omega_c}\right) \ , \ \kappa(\Delta_{kj}) = \kappa_0 \frac{\Delta_{kj}}{\omega} \exp\left(-\frac{\Delta_{kj}}{\omega_c}\right) \ , \tag{1.40}$$

where we set the cut-off frequencies $\Omega_c = 10\Omega$ and $\omega_c = 10\omega$.

By solving the system $\dot{\mathbf{Y}} = \mathbf{M}\mathbf{Y}$, one obtains all the coefficients $r_{N,M}$ as function of time. Once they are found, it is simpler to calculate the average values of observables by rewriting the density operator in the form of Eq. (1.6). From the dressed-state expansion (1.36), one finds

$$A_{NM} = \sum_{n,m=0}^{Q_2} r_{n,m} c_{N,n} c_{M,m}^* \tag{1.41}$$

$$B_{NM} = \sum_{n,m=0}^{Q_2} r_{n,m} c_{N+Q_1+1,n} c_{M+Q_1+1,m}^* \tag{1.42}$$

$$C_{NM} = \sum_{n,m=0}^{Q_2} r_{n,m} c_{N,n} c_{M+Q_1+1,m}^* \ . \tag{1.43}$$

The initial conditions for the coefficients r_{nm} are found as follows. For the initial state with the atom in the ground state,

$$\rho_0 = |g\rangle\langle g| \otimes \sum_{N,M=0}^{Q_1} p_{N,M} |f_N\rangle\langle f_M| \tag{1.44}$$

one obtains

$$r_{n,m}(0) = \sum_{i,j=0}^{Q_1} p_{i,j} c^*_{i+1,n} c_{j+1,m} \ . \tag{1.45a}$$

On the other hand, if it was initially in the excited state, then

$$r_{n,m}(0) = \sum_{i,j=0}^{Q_1} p_{i,j} c^*_{i+Q_1+2,n} c_{j+Q_1+2,m} \ . \tag{1.46}$$

In this work, we assume that the atom is initially in the ground state.

Finally, for a pure initial cavity state, we write $\rho_c(0) = |\psi(0)\rangle\langle\psi(0)|$, where

$$|\psi(0)\rangle = \sum_{n=0}^{Q_1} \chi_n |n\rangle \ . \tag{1.47}$$

In Sections 1.5 – 1.8 we will describe how to find the recurrence relations for χ_n for some common states.

1.4.1 DME in the bare basis

When the Rabi Hamiltonian depends explicitly on time and the dissipation is weak, for accuracy reasons it is advantageous to expand the density operador in terms of the bare basis, as in Eq. (1.6). Then, after straightforward calculations, one gets for $1 \leq N, M \leq Q_1 + 1$

$$\begin{aligned} \dot{A}_{NM} &= \text{unitary part} + \sum_{n,m=1}^{Q_1+1} [W^{(N,M,n,m)}_{A,A} A_{nm} + W^{(N,M,n,m)}_{A,B} B_{nm} \\ &\quad + W^{(N,M,n,m)}_{A,C} C_{nm} + W^{(N,M,n,m)}_{A,D} C^*_{mn}] \end{aligned} \tag{1.48}$$

$$\begin{aligned} \dot{B}_{NM} &= \text{unitary part} + \sum_{n,m=1}^{Q_1+1} [W^{(N,M,n,m)}_{B,A} A_{nm} + W^{(N,M,n,m)}_{B,B} B_{nm} \\ &\quad + W^{(N,M,n,m)}_{B,C} C_{nm} + W^{(N,M,n,m)}_{B,D} C^*_{mn}] \end{aligned} \tag{1.49}$$

$$\begin{aligned} \dot{C}_{NM} &= \text{unitary part} + \sum_{n,m=1}^{Q_1+1} [W^{(N,M,n,m)}_{C,A} A_{nm} + W^{(N,M,n,m)}_{C,B} B_{nm} \\ &\quad + W^{(N,M,n,m)}_{C,C} C_{nm} + W^{(N,M,n,m)}_{C,D} C^*_{mn}] \end{aligned} \tag{1.50}$$

where the unitary part as the same as in Eqs. (1.23) – (1.25) (i.e., setting $\kappa_0 = \gamma_0 = \gamma_\phi = 0$) , while the dissipative contributions are:

$$W_{A,A}^{(N,M,n,m)} = \sum_{j,k=0}^{Q_2} \Phi_j \Phi_k c_{n,j}^* c_{m,k} c_{N,j} c_{M,k}^* \tag{1.51}$$

$$-\delta_{m,M} \frac{1}{2} \sum_{k=0}^{Q_2} \Phi_k^2 c_{N,k} c_{n,k}^* - \delta_{n,N} \frac{1}{2} \sum_{k=0}^{Q_2} \Phi_k^2 c_{M,k}^* c_{m,k} \tag{1.52}$$

$$+ \sum_{j=0}^{Q_2-1} \sum_{k=j+1}^{Q_2} \Gamma^{jk} \left[c_{N,j} c_{M,j}^* c_{n,k}^* c_{m,k} - \frac{1}{2} \delta_{m,M} c_{N,k} c_{n,k}^* - \frac{1}{2} \delta_{n,N} c_{m,k} c_{M,k}^* \right]$$

$$W_{A,B}^{(N,M,n,m)} = \sum_{j,k=0}^{Q_2} \Phi_j \Phi_k c_{n+Q_1+1,j}^* c_{m+Q_1+1,k} c_{N,j} c_{M,k}^* \tag{1.53}$$

$$+ \sum_{j=0}^{Q_2-1} \sum_{k=j+1}^{Q_2} \Gamma^{jk} \left[c_{N,j} c_{M,j}^* c_{n+Q_1+1,k}^* c_{m+Q_1+1,k} \right]$$

$$W_{A,C}^{(N,M,n,m)} = \sum_{j,k=0}^{Q_2} \Phi_j \Phi_k c_{n,j}^* c_{m+Q_1+1,k} c_{N,j} c_{M,k}^* - \delta_{n,N} \frac{1}{2} \sum_{k=0}^{Q_2} \Phi_k^2 c_{M,k}^* c_{m+Q_1+1,k}$$

$$+ \sum_{j=0}^{Q_2-1} \sum_{k=j+1}^{Q_2} \Gamma^{jk} \left[c_{N,j} c_{M,j}^* c_{n,k}^* c_{m+Q_1+1,k} - \delta_{n,N} \frac{1}{2} c_{m+Q_1+1,k} c_{M,k}^* \right] \tag{1.54}$$

$$W_{B,A}^{(N,M,n,m)} = \sum_{j,k=0}^{Q_2} \Phi_j \Phi_k c_{N+Q_1+1,j} c_{M+Q_1+1,k}^* c_{n,j}^* c_{m,k} \tag{1.55}$$

$$+ \sum_{j=0}^{Q_2-1} \sum_{k=j+1}^{Q_2} \Gamma^{jk} \left[c_{N+Q_1+1,j} c_{M+Q_1+1,j}^* c_{n,k}^* c_{m,k} \right]$$

$$W_{B,B}^{(N,M,n,m)} = \sum_{j,k=0}^{Q_2} \Phi_j \Phi_k c_{N+Q_1+1,j} c_{M+Q_1+1,k}^* c_{n+Q_1+1,j}^* c_{m+Q_1+1,k} \tag{1.56}$$

$$-\delta_{m,M} \frac{1}{2} \sum_{k=0}^{Q_2} \Phi_k^2 c_{N+Q_1+1,k} c_{n+Q_1+1,k}^* - \delta_{n,N} \frac{1}{2} \sum_{k=0}^{Q_2} \Phi_k^2 c_{M+Q_1+1,k}^* c_{m+Q_1+1,k}$$

$$+ \sum_{j=0}^{Q_2-1} \sum_{k=j+1}^{Q_2} \Gamma^{jk} \left[c_{N+Q_1+1,j} c_{M+Q_1+1,j}^* c_{n+Q_1+1,k}^* c_{m+Q_1+1,k} \right.$$

$$\left. -\delta_{m,M} \frac{1}{2} c_{N+Q_1+1,k} c_{n+Q_1+1,k}^* - \delta_{n,N} \frac{1}{2} c_{M+Q_1+1,k}^* c_{m+Q_1+1,k} \right]$$

$$W_{B,C}^{(N,M,n,m)} = \sum_{j,k=0}^{Q_2} \Phi_j \Phi_k c_{N+Q_1+1,j} c^*_{M+Q_1+1,k} c^*_{n,j} c_{m+Q_1+1,k} - \delta_{m,M} \frac{1}{2} \sum_{k=0}^{Q_2} \Phi_k^2 c_{N+Q_1+1,k} c^*_{n,k}$$
$$+ \sum_{j=0}^{Q_2-1} \sum_{k=j+1}^{Q_2} \Gamma^{jk} \left[c_{N+Q_1+1,j} c^*_{M+Q_1+1,j} c^*_{n,k} c_{m+Q_1+1,k} - \delta_{m,M} \frac{1}{2} c_{N+Q_1+1,k} c^*_{n,k} \right] \quad (1.57)$$

$$W_{B,D}^{(N,M,n,m)} = \sum_{j,k=0}^{Q_2} \Phi_j \Phi_k c_{N+Q_1+1,j} c^*_{M+Q_1+1,k} c^*_{n+Q_1+1,j} c_{m,k} - \delta_{n,N} \frac{1}{2} \sum_{k=0}^{Q_2} \Phi_k^2 c^*_{M+Q_1+1,k} c_{m,k}$$
$$+ \sum_{j=0}^{Q_2-1} \sum_{k=j+1}^{Q_2} \Gamma^{jk} \left[c_{N+Q_1+1,j} c^*_{M+Q_1+1,j} c^*_{n+Q_1+1,k} c_{m,k} - \delta_{n,N} \frac{1}{2} c^*_{M+Q_1+1,k} c_{m,k} \right] \quad (1.58)$$

$$W_{C,A}^{(N,M,n,m)} = \sum_{j,k=0}^{Q_2} \Phi_j \Phi_k c_{N,j} c^*_{M+Q_1+1,k} c^*_{n,j} c_{m,k} - \delta_{n,N} \sum_{k=0}^{Q_2} \frac{1}{2} \Phi_k^2 c^*_{M+Q_1+1,k} c_{m,k}$$
$$+ \sum_{j=0}^{Q_2-1} \sum_{k=j+1}^{Q_2} \Gamma^{jk} \left[c_{N,j} c^*_{M+Q_1+1,j} c^*_{n,k} c_{m,k} - \delta_{n,N} \frac{1}{2} c^*_{M+Q_1+1,k} c_{m,k} \right] \quad (1.59)$$

$$W_{C,B}^{(N,M,n,m)} = \sum_{j,k=0}^{Q_2} \Phi_j \Phi_k c_{N,j} c^*_{M+Q_1+1,k} c^*_{n+Q_1+1,j} c_{m+Q_1+1,k}$$
$$- \delta_{m,M} \sum_{k=0}^{Q_2} \frac{1}{2} \Phi_k^2 c_{N,k} c^*_{n+Q_1+1,k} \quad (1.60)$$
$$+ \sum_{j=0}^{Q_2-1} \sum_{k=j+1}^{Q_2} \Gamma^{jk} \left[c_{N,j} c^*_{M+Q_1+1,j} c^*_{n+Q_1+1,k} c_{m+Q_1+1,k} - \delta_{M,m} \frac{1}{2} c_{N,k} c^*_{n+Q_1+1,k} \right]$$

$$W_{C,C}^{(N,M,n,m)} = \sum_{j,k=0}^{Q_2} \Phi_j \Phi_k c_{N,j} c^*_{M+Q_1+1,k} c^*_{n,j} c_{m+Q_1+1,k} - \delta_{m,M} \frac{1}{2} \sum_{k=0}^{Q_2} \Phi_k^2 c_{N,k} c^*_{n,k}$$
$$- \delta_{N,n} \sum_{k=0}^{Q_2} \frac{1}{2} \Phi_k^2 c^*_{M+Q_1+1,k} c_{m+Q_1+1,k} \quad (1.61)$$
$$+ \sum_{j=0}^{Q_2-1} \sum_{k=j+1}^{Q_2} \Gamma^{jk} \left[c_{N,j} c^*_{M+Q_1+1,j} c^*_{n,k} c_{m+Q_1+1,k} \right.$$
$$\left. - \delta_{m,M} \frac{1}{2} c_{N,k} c^*_{n,k} - \delta_{n,N} \frac{1}{2} c^*_{M+Q_1+1,k} c_{m+Q_1+1,k} \right]$$

$$W_{C,D}^{(N,M,n,m)} = \sum_{j,k=0}^{Q_2} \Phi_j \Phi_k c_{N,j} c_{M+Q_1+1,k}^* c_{n+Q_1+1,j}^* c_{m,k} + \sum_{j=0}^{Q_2-1} \sum_{k=j+1}^{Q_2} \Gamma^{jk} \left[c_{N,j} c_{M+Q_1+1,j}^* c_{n+Q_1+1,k}^* c_{m,k} \right] \tag{1.62}$$

When the parameters of the Hamiltonian, and hence the dressed-states, depend explicitly on time, we make the simplifying assumption that the modulations and the dissipation are weak, so in evaluating the dressed states one can use the unperturbed values of the parameters. This is plausible when the modulation of the parameter X is of the form $X(t) = X_0 [1 + \varepsilon f(t)]$, where $|f(t)| \leq 1$ is some time-dependent function and $\varepsilon \ll 1$ is the modulation amplitude. Moreover, to make the system of ODE numerically treatable, we make an additional approximation whereby we set $W_{X,Y}^{(N,M,n,m)} = 0$ whenever $\left| W_{X,Y}^{(N,M,n,m)} \right| < \epsilon$, where ϵ is the threshold parameter and X and Y stand for A, B, C and D. This is reasonable when the dissipation acts as a perturbation to the coherent dynamics, when all the dissipation rates are much smaller that the atom–field coupling strength g.

1.5 Coherent state

For the coherent state $|\alpha\rangle$ with a real amplitude α, we have

$$|\alpha\rangle = e^{-\alpha^2/2} \sum_{n=0}^{\infty} \frac{\alpha^2}{\sqrt{n!}} |n\rangle \ . \tag{1.63}$$

The recurrence relations read

$$\chi_0 = \exp\left(-\frac{\alpha^2}{2}\right) \ , \ \chi_{n+1} = \chi_n \frac{\alpha}{\sqrt{n+1}} \ . \tag{1.64}$$

Figures 1.1, 1.2 and 1.3 show the dynamics of the atomic excitation probability, $P_e = \mathrm{Tr}\left[\rho |e\rangle\langle e|\right]$, average photon number, $\langle n \rangle = \mathrm{Tr}\left[\rho a^\dagger a\right]$, Mandel Q-factor

$$Q = \frac{\left\langle (\Delta n)^2 \right\rangle - \langle n \rangle}{\langle n \rangle} \ , \tag{1.65}$$

qubit and cavity purities [Eqs. (1.9) and (1.10)], negativity [Eq. 1.11], and the photon number probability distribution for three different time instants. The parameters were chosen to correspond, approximately, to the three-, five- and seven-photon resonances, as will be explained in Section 1.10 (note that the exact resonances are photon number dependent [29–32]).

First of all, we can observe that the GKSL ME (blue lines) predicts much faster damping of the fast oscillations (due to the exchange of excitations between the qubit and the field), which on the considered time interval are perceived as a large width of the curves. Besides, DME for both ohmic and white spectral densities predict much faster decay of the purities and negativity.This observation seems to agree with the conclusion of

[22] that in the dispersive regime DME overestimates the effects of relaxation. Moreover, the predictions of the three models for P_e, $\langle n\rangle$ and Q do not coincide for large times, $gt \gg 1$, meaning that the accurate description of the system requires a precise knowledge of the spectral density in order to use an appropriate master equation.

1.6 Odd Schrödinger cat state

The odd Schrödinger cat state [33] is defined in terms of the coherent states with opposite amplitudes as

$$|\psi\rangle = \frac{|\alpha\rangle - |-\alpha\rangle}{\sqrt{2-2e^{-2\alpha^2}}} \ , \tag{1.66}$$

where for brevity we consider that α is a real parameter. The recurrence relations are:

$$\chi_0 = 0 \ , \ \chi_1 = \sqrt{\frac{2}{1-e^{-2\alpha^2}}}\alpha e^{-\alpha^2/2} \ , \ \chi_{n+2} = \chi_n \frac{\alpha^2}{\sqrt{(n+2)(n+1)}} \, . \tag{1.67}$$

The results for the Schrödinger cat states with the initial average photon number $\langle n(0)\rangle = 50$ (corresponding to $\alpha = 7.071$) and coupling constants $g = 0.1\omega$, 0.3ω and 0.5ω are shown in Figures 1.4 – 1.6. We see that the predictions of the different dissipative models for the quantities P_e, $\langle n\rangle$ and Q are similar (although DME predicts faster relaxation of the coherences). On the other hand, for the quantities $\mathcal{N}$, Π_{qubit} and Π_{field}, as well as the photon number statistics, the differences may be substantial, depending on the parameters and the time interval.

1.7 Squeezed coherent state

For the real parameters s and β, the probability amplitude of the squeezed coherent state $|s,\beta\rangle$ is

$$\chi_n = \exp\left[-\frac{\beta^2}{2}(1-\tanh s)\right]\frac{1}{\sqrt{n!\cosh s}}\left(\frac{\tanh s}{2}\right)^{n/2} H_n(x) \ , \tag{1.68}$$

where $H_n(x)$ is the Hermite polynomial and $x = \beta/\sqrt{\sinh 2s}$ [1, 3, 5, 33]. The recurrence relations are

$$\chi_0 = \exp\left[-\frac{1}{2}\beta^2(1-\tanh s)\right]\frac{1}{\sqrt{\cosh s}} \ , \ \chi_{n+1} = \chi_n K_n(x)\sqrt{\frac{\tanh s}{2(n+1)}} \, . \tag{1.69}$$

Here we defined $K_n(x) \equiv H_{n+1}(x)/H_n(x)$, and from the well known recurrence relations for the Hermite polynomials, one has

$$K_0(x) = 2x \ , \ K_{n+1}(x) = 2x - \frac{2(n+1)}{K_n(x)} \, . \tag{1.70}$$

The results for the initial average photon number $\langle n\,(0)\rangle = 50$ (corresponding to $s = 0.7$ and $\beta = 14.157$) and coupling constants $g = 0.1\omega$, 0.3ω and 0.5ω are shown in Figures 1.7 – 1.9. From the plots we obtain, similar conclusions to the ones in Section 1.6.

1.8 Squeezed vacuum state

If $\beta = 0$, the recurrence relations (1.69) become

$$\chi_0 = \frac{1}{\sqrt{\cosh s}}\ ,\ \chi_1 = 0\ ,\ \chi_{m+2} = -\chi_m\sqrt{\frac{m+1}{m+2}}\tanh s\ . \tag{1.71}$$

We show the results for the initial state with $\langle n\,(0)\rangle = 5$ (corresponding to the squeezing parameter $s = 1.544$) in Figures 1.10 (for $g = 0.5\omega$, $\Omega = 1.5\omega$) and 1.11 (for $g = 0.8\omega$, $\Omega = 2.9\omega$), assuming relatively strong dissipative rates $\kappa_0 = \gamma_0 = \gamma_{ph} = 10^{-3}\omega$. In all these examples, the discrepancies between the three dissipative models are substantial, therefore an accurate description of the system dynamics require a precise knowledge of the spectral density of the reservoir.

1.9 Thermal state

For the thermal state, which is a mixed state, the cavity density operator is

$$\rho_c\,(0) = \sum_{n=0}^{\infty}\chi_n|n\rangle\langle n|\ ,\ \chi_n = \frac{\alpha^n}{(\alpha+1)^{n+1}}\ , \tag{1.72}$$

where α is the average number of photons. The recurrence relations are

$$\chi_0 = \frac{1}{\alpha+1}\ ,\ \chi_{n+1} = \chi_n\frac{\alpha}{\alpha+1}\ , \tag{1.73}$$

while the initial condition (1.45a) becomes

$$r_{n,m}\,(0) = \sum_{i=0}^{Q_1}\chi_i c^*_{i+1,n}c_{i+1,m}\,. \tag{1.74}$$

The system behavior for $\alpha = 5$ and other parameters as in Figures 1.10 – 1.11 is illustrated in Figures 1.12 – 1.13. As in Section 1.8, the discrepancies between the predictions of the dissipative models are significant for all the considered quantities.

1.10 Multi-photon Rabi oscillations

Now we consider the initial state $|e,0\rangle$ and study the deexcitation of the qubit via 3-, 5- and 7-photon processes, which are intrinsic to both the quantum and semiclassical Rabi Hamiltonian due to the counter-rotating terms [29–32, 34–37]. In Figure 1.14 we consider the three-photon resonance (betweem the states $|e,0\rangle$ and $|g,3\rangle$) for the parameters $g = 0.1\omega$, $\Omega = 2.9699\omega$ and the dissipative rates $\kappa_0 = \gamma_0 = \gamma_{ph} = 10^{-5}\omega$. By plotting the same quantities as in the previous figures, we see that the predictions of the three dissipative models are very close, although the DME predicts a slightly faster decay of the coherences (as in the previous cases). Moreover, panels 1.14g – 1.14i confirm that the deexcitation of the qubit populates the cavity mostly in the 3-photon Fock state.

Figures 1.15 and 1.16 illustrate the system behavior for the 5- and 7-photon resonances (for the state $|e,0\rangle$) and larger light-matter coupling strengths. We maintained the same dissipative rates as in Figure 1.14 and set the other parameters as: $g = 0.3\omega$, $\Omega = 4.7736\omega$ (5-photon resonance) and $g = 0.5\omega$, $\Omega = 6.4121\omega$ (7-photon resonance). As expected, the discrepancies in the predictions of different dissipative models become more pronounced with the increase of g, although the qualitative behavior remains similar.

1.11 Nonstationary Rabi Hamiltonian with post-selection

Finally, we consider photon generation from the initial vacuum state $|g,0\rangle$ induced by modulation of the system parameters, in analogy with the dynamical Casimir effect. We assume a modulation of the qubit transition frequency,

$$\Omega(t) = \Omega_0 \left\{1 + \varepsilon \sin[\eta(t)t]\right\} \ , \tag{1.75}$$

where Ω_0 is the bare qubit frequency, $\varepsilon \ll \Omega_0$ is the relative modulation amplitude, and $\eta(t)$ is the time-dependent modulation frequency. Following the proposal of Ref. [38], we consider a slow linear sweep, $\eta(t) = \eta_0 + \alpha t$, where η_0 and α are constant parameters.

Our first objective is to compare the predictions of the DME and the GKSL ME for the parameter regime analyzed in Ref. [38], since the DME was not considered in that work. The second objective is to investigate the effect of post-selecting the final cavity-field state conditioned on detecting the qubit in the ground state. In this case, the cavity-field density operator at time t becomes

$$\rho_{PS}(t) = \frac{\mathrm{Tr}_q\left(|g\rangle\langle g|\rho(t)\right)}{\mathrm{Tr}\left(|g\rangle\langle g|\rho(t)\right)} \ , \tag{1.76}$$

where $\rho(t)$ is the total density operator of the qubit–cavity system.

Ref. [38] showed that the generated cavity-field states may find applications in quantum metrology. Without entering into detailed derivations, we evaluate here the quantity known as the *quantum Fisher information* (QFI) for phase estimation under unitary

encoding. As discussed in several reviews [39–42], it is given by

$$\mathcal{F}_{ph} = \frac{1}{2}\sum_{i,j}\frac{\left(p_i - p_j\right)^2}{p_i + p_j}\left|\langle i|\hat{n}|j\rangle\right|^2 , \tag{1.77}$$

where p_i and $|i\rangle$ are the eigenvalues and eigenvectors of $\rho_{PS}(t)$. Any quantum state satisfying $\mathcal{F}_{ph} > \langle n\rangle$, where $\langle n\rangle$ denotes the mean photon number of the state, possesses metrological advantage over any classical state of light.

In addition, for the estimation of a *phase-space displacement* of a single-mode field, one must consider the 2×2 quantum Fisher information matrix with elements

$$\left(F_{disp}\right)_{kl} = \sum_{i,j}\frac{\left(p_i - p_j\right)^2}{p_i + p_j}\langle i|x^{(k)}|j\rangle\langle j|x^{(l)}|i\rangle , \tag{1.78}$$

where $x^{(1)} = a + a^\dagger$ and $x^{(2)} = \left(a - a^\dagger\right)/i$. The *average Fisher information* over all quadrature directions is

$$M_{av} = \frac{1}{4}\mathrm{Tr}\left(\mathbf{F}_{disp}\right) , \tag{1.79}$$

while the *maximum Fisher information* is

$$M_{opt} = \frac{1}{2}\lambda_{\max}\left(\mathbf{F}_{disp}\right) , \tag{1.80}$$

where $\lambda_{\max}\left(\mathbf{F}_{disp}\right)$ denotes the largest eigenvalue of $\mathbf{F}_{disp}$. Any quantum state satisfying $M_{av}(\rho_{PS}) > 1$ or $M_{opt}(\rho_{PS}) > 1$ exhibits metrological advantage for displacement estimation compared to classical states of light.

We solved numerically the DME and the GKSL ME for the parameters used in Ref. [38] and found that for initial times, $\omega t \lesssim 2\times 10^4$, the predictions of the three dissipative models are nearly indistinguishable (data not shown for brevity), thereby supporting the validity of the results reported in Ref. [38], where only the GKSL ME was employed. To present new results and highlight differences between the dissipative approaches, panels 1.17a and 1.18a display the excited-state probability of the qubit for modulations inducing two- and four-photon transitions, respectively. Since $P_g \gtrsim 0.5$ at all times, post-selection of the cavity field conditioned on detecting the qubit in the ground state $|g\rangle$ remains experimentally feasible. We therefore analyze the properties of the post-selected cavity state.

Specifically, we evaluate the mean photon number, the Mandel Q-factor, the metrological quantities (1.77), (1.79), and (1.80), as well as the photon-number probability distribution at selected time instants. For early times, $\omega t \lesssim 2\times 10^4$, the predictions of the three dissipative models are nearly identical in these weak-dissipation regimes, even for ultrastrong coupling $g = 0.15\omega$. At later times, the predictions of the DME remain very similar for white and Ohmic reservoirs, but start to deviate quantitatively from those of the GKSL master equation. Furthermore, at longer times, the post-selected cavity-field states exhibit a clear metrological advantage and feature a photon-number distribution with a highly nontrivial, nonmonotonic structure, including a pronounced tail at large n.

1.12 Summary

In this chapter, we have presented a detailed numerical investigation of the dissipative dynamics of the quantum Rabi model in the ultrastrong coupling regime, considering several paradigmatic states of quantum optics: coherent, Schrödinger cat, squeezed, thermal, and vacuum states. We explored different detunings and coupling strengths in the range 0.05ω to 0.8ω, including multiphoton resonance regimes. The analysis focused on the time evolution of key observables such as the atomic excitation probability, mean photon number, Mandel Q-factor, negativity, purities, and photon-number probability distributions. We also examined the regime of external time-dependent modulation of the qubit parameters [38], where multiphoton processes enable photon generation from the vacuum via two- and four-photon transitions. In this context, we demonstrated that postselection protocols can be employed to engineer and tailor the properties of the cavity field.

Our results reveal that, in certain parameter regimes, the predictions of the standard GKSL master equation (ME) and the dressed master equation (DME) differ substantially across all observables considered. In other regimes, however, the two approaches lead to qualitatively similar dynamics for some quantities while exhibiting noticeable quantitative differences for others. Consistent with previous observations [22], we find that in the dispersive regime the DME tends to predict stronger coherence losses: high-frequency oscillations superimposed on the primary dynamical envelope are more heavily damped, and quantities such as purities and negativity decay faster than in the GKSL treatment. Nevertheless, without resorting to the generalized dressed master equation, it is not possible to state definitively that such an overestimation occurs universally.

The main conclusion of this work is therefore methodological as well as physical. When investigating new parameter regimes of the ultrastrong-coupling Rabi model, both the GKSL ME and the DME should be solved numerically and compared carefully, possibly using computational strategies such as those illustrated here. At the same time, for the parameter ranges analyzed in this chapter, our extensive numerical results provide a practical reference for anticipating both the qualitative trends and quantitative deviations associated with each master-equation approach.

1.13 Acknowledgments

A.P.C acknowledges the financial support by the Brazilian agency Coordenação de Aperfeiçoamento de Pessoal de Nível Superior (CAPES, Finance Code 001). H.S.R.O. acknowledges the financial support of the Brazilian agency Fundação de Apoio à Pesquisa do Distrito Federal (FAPDF, program PIBIC). A. D. acknowledges a partial financial support of the Brazilian agency Fundação de Apoio à Pesquisa do Distrito Federal (FAPDF, grant number 00193-00001817/2023-43).

1.14 References

[1] M. O. Scully and M. S. Zubairy, *Quantum Optics* (Cambridge University Press, Cambridge, 1997).

[2] H. Carmichael, *An Open System Approach to Quantum Optics* (Springer, Berlin, 1993).

[3] W. Vogel and D. -G. Welsch, *Quantum Optics* (Wiley, Berlin, 2006).
[4] H. -P. Breuer and F. Petruccione, *The theory of open quantum systems* (Oxford University Press, Oxford, 2002).
[5] M. Orszag, *Quantum Optics* (Springer, Berlin, 2nd Edition, 2008).
[6] C. Gonzalez-Ballestero, Tutorial: projector approach to master equations for open quantum systems, Quantum **8**, 1454 (2024).
[7] I. de Vega and D. Alonso, Dynamics of non-Markovian open quantum systems, Rev. Mod. Phys. **89**, 015001 (2017).
[8] T. Niemczyk, F. Deppe, H. Huebl, E. P. Menzel, F. Hocke, M. J. Schwarz, J. J. Garcia-Ripoll, D. Zueco, T. Hümmer, E. Solano, A. Marx, and R. Gross, Circuit quantum electrodynamics in the ultrastrong-coupling regime, Nat. Phys. **6**, 772 (2010).
[9] A. F. Kockum, A. Miranowicz, S. De Liberato, S. Savasta, and F. Nori, Ultrastrong coupling between light and matter, Nat. Rev. Phys. **1**, 19 (2019).
[10] P. Forn-Díaz, L. Lamata, E. Rico, J. Kono, and E. Solano, Ultrastrong coupling regimes of light-matter interaction, Rev. Mod. Phys. **91**, 025005 (2019).
[11] W. Qin, A. F. Kockum, C. S. Muñoz, A. Miranowicz, and F. Nori, Quantum amplification and simulation of strong and ultrastrong coupling of light and matter, Phys. Rep. **1078**, 1 (2024).
[12] T. Werlang, A. V. Dodonov, E. I. Duzzioni, and C. J. Villas Boas, Rabi model beyond the rotating-wave approximation: Generation of photons from vacuum through decoherence, Phys. Rev. A **78**, 053805 (2008).
[13] S. De Liberato, D. Gerace, I. Carusotto, and C. Ciuti, Extracavity quantum vacuum radiation from a single qubit, Phys. Rev. A **80**, 053810 (2009)
[14] F. Beaudoin, J. M. Gambetta and A. Blais, Dissipation and ultrastrong coupling in circuit QED, Phys. Rev. A **84**, 043832 (2011).
[15] I. I. Rabi. On the Process of Space Quantization. Phys. Rev. **49**, 324 (1936).
[16] I. I. Rabi. Space quantization in a gyrating magnetic field. Phys. Rev. **51**, 652 (1937).
[17] D. Braak. Integrability of the Rabi model. Phys. Rev. Lett. **107**, 100401 (2011).
[18] Q. Xie, H. Zhong, M. T Batchelor and C. Lee, The quantum Rabi model: solution and dynamics. J. Phys. A.: Math. Theor. **50**, 113001 (2017).
[19] J. Larson and Th. K. Mavrogordatos, *The Jaynes-Cummings Model and Its Descendants* (IOP Publishing, Bristol, 2021). https://arxiv.org/abs/2202.00330 (2024).
[20] S. Agarwal, S. M. Hashemi Rafsanjani and J. H. Eberly, Dissipation of the Rabi model beyond the Jaynes–Cummings approximation: quasi-degenerate qubit and ultra-strong coupling, J. Phys. B: At. Mol. Opt. Phys. **46**, 224017 (2013).
[21] M. Bamba and T. Ogawa, Recipe for the Hamiltonian of system-environment coupling applicable to the ultrastrong-light-matter-interaction regime, Phys. Rev. A **89**, 023817 (2014).
[22] A. Settineri, V. Macrì, A. Ridolfo, O. Di Stefano, A. F. Kockum, F. Nori, and S. Savasta, Dissipation and thermal noise in hybrid quantum systems in the ultrastrong-coupling regime, Phys. Rev. A **98**, 053834 (2018).
[23] W. Salmon, C. Gustin, A. Settineri, O. Di Stefano, D. Zueco, S. Savasta, F. Nori and S. Hughes, Gauge-independent emission spectra and quantum correlations in the ultrastrong coupling regime of open system cavity-QED, Nanophotonics **11**, 1573 (2022).
[24] A. Trushechkin, Quantum master equations and steady states for the ultrastrong-

coupling limit and the strong-decoherence limit, Phys. Rev. A **106**, 042209 (2022).
[25] M. Lednev, F. J. García-Vidal and J. Feist, Lindblad master equation capable of describing hybrid quantum systems in the ultrastrong coupling regime, Phys. Rev. Lett. **132**, 106902 (2024).
[26] Y. Tanimura, Numerically "exact" approach to open quantum dynamics: The hierarchical equations of motion (HEOM), J. Chem. Phys. **153**, 020901 (2020).
[27] G. Vidal and R.F. Werner, Computable measure of entanglement, Phys. Rev. A **65**, 032314 (2002).
[28] A. Ridolfo, M. Leib, S. Savasta, and M. J. Hartmann, Photon Blockade in the Ultrastrong Coupling Regime, Phys. Rev. Lett. **109**, 193602 (2012).
[29] A. Marinho, M.V.S. de Paula and A.V. Dodonov, Approximate analytic solution of the dissipative semiclassical Rabi model near the three-photon resonance and comparison with the quantum behavior, Phys. Lett. A **513**, 129608 (2024).
[30] M. V. S. de Paula, M. A. Damasceno Faustino and A. V. Dodonov, A Comparison of Quantum and Semiclassical Rabi Models Near Multiphoton Resonances in the Presence of Parametric Modulation, Physics **7**, 42 (2025).
[31] A. P. Costa and A. Dodonov, Quantum Rabi oscillations in the semiclassical limit: backreaction on the cavity field and entanglement, in A. Dodonov and L. C. Céleri (Eds.), Proceedings – QNS III International Workshop on Quantum Nonstationary Systems, pp. 71-88 (LF Editorial, São Paulo, 2025). DOI: 10.29327/5559166.
[32] A. P. Costa and A. Dodonov, One- and multiphoton resonances in the light-atom interaction, Revista Brasileira de Ensino de Física **47**, e20250251 (2025).
[33] C. C. Gerry and P. L. Knight, *Introductory Quantum Optics* (Cambridge University Press, Cambridge, 2005).
[34] A.B. Klimov, I. Sainz, S.M. Chumakov, Resonance expansion versus the rotating-wave approximation, Phys. Rev. A **68**, 063811 (2003).
[35] K.K.W. Ma, C.K. Law, Three-photon resonance and adiabatic passage in the large-detuning Rabi model, Phys. Rev. A **92**, 023842 (2015).
[36] L. Garziano, R. Stassi, V. Macrì, A.F. Kockum, S. Savasta, F. Nori, Multiphoton quantum Rabi oscillations in ultrastrong cavity QED, Phys. Rev. A **92**, 063830 (2015).
[37] L. Cong, S. Felicetti, J. Casanova, L. Lamata, E. Solano, I. Arrazola, Selective interactions in the quantum Rabi model, Phys. Rev. A **101**, 032350 (2020).
[38] H. R. Schelb, A. P. Costa and A. V. Dodonov, Metrological power of single-qubit dynamical Casimir effect in circuit QED, Phys. Lett. A **566**, 131163 (2026).
[39] D. Petz and C. Ghinea, Introduction to Quantum Fisher Information, Quantum Probability and Related Topics, 261-281 (2011). DOI: 10.1142/9789814338745_0015
[40] G. Tóth and I. Apellaniz, Quantum metrology from a quantum information science perspective, J. Phys. A: Math. Theor. **47**, 424006 (2014).
[41] K.C. Tan and H. Jeong, Nonclassical Light and Metrological Power: An Introductory Review, AVS Quantum Sci. **1**, 014701 (2019).
[42] J.S. Sidhu and P. Kok, A Geometric Perspective on Quantum Parameter Estimation, AVS Quantum Sci. **2**, 014701 (2020).

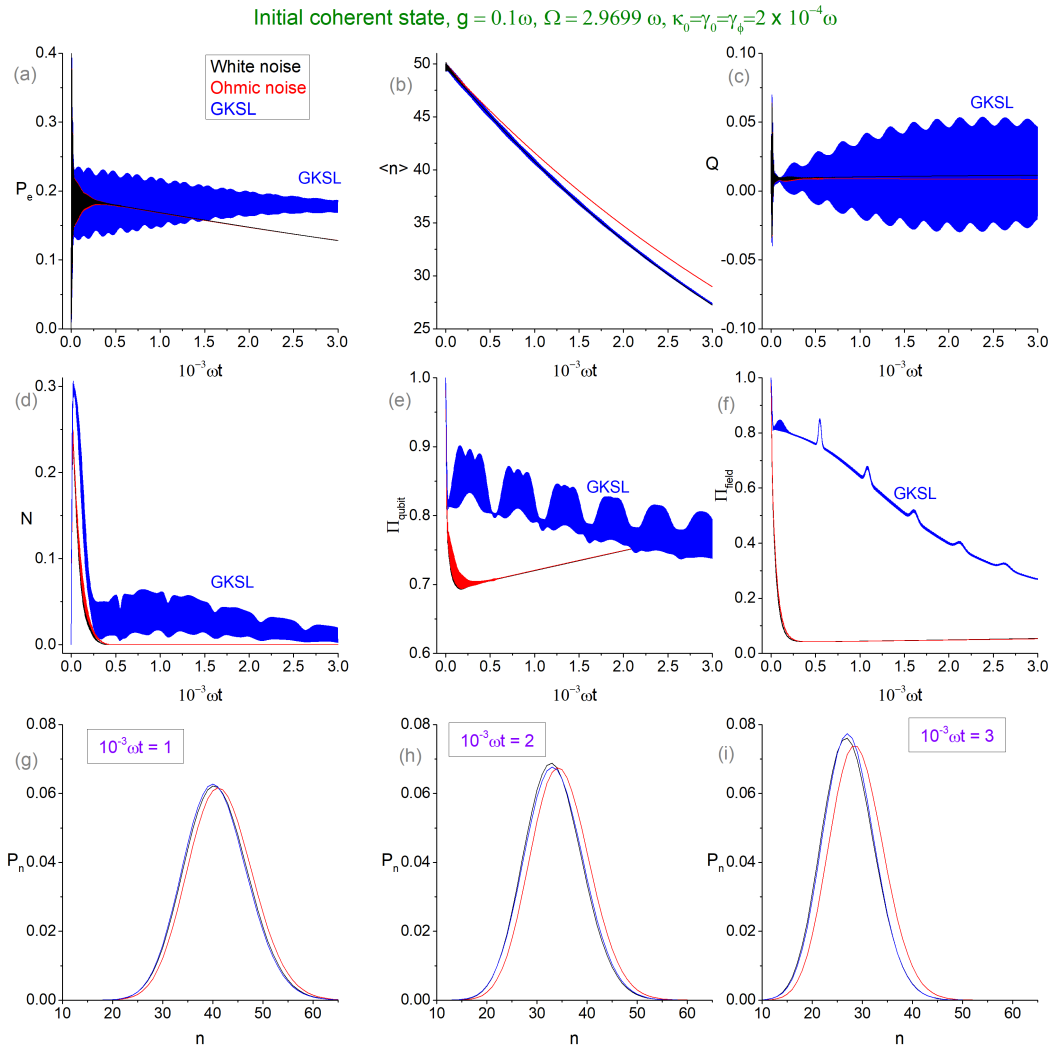

Figure 1.1: Behavior of the quantum Rabi model under dissipation for the initial coherent state, Eq. (1.63), and parameters $\alpha = \sqrt{50}$, $g = 0.1\omega$, $\Omega = 2.9699\omega$ and $\kappa_0 = \gamma_0 = \gamma_\phi = 2 \times 10^{-4}\omega$. In all the figures of this chapter it is assumed that the qubit was initially in the ground state. a) Qubit excitation probability. b) Average photon number. c) Mandel's Q-factor. d) Negativity (nonzero values attest qubit-field entanglement). e) Qubit's purity. f) Field's purity. g) Photon number probability distribution at the instant of time $\omega t = 10^3$. h) Photon number probability distribution at the instant of time $\omega t = 2 \times 10^3$. i) Photon number probability distribution at the instant of time $\omega t = 3 \times 10^3$. Blue lines correspond to the predictions of the GKSL ME, black lines – to the predictions of the dressed-picture ME for white noise and red lines – to the predictions of the dressed-picture ME for ohmic noise. Whenever the predictions of the GKSL master equation differ significantly from those of the DME, the corresponding curves are explicitly labeled as "GKSL" in the plots for improved clarity.

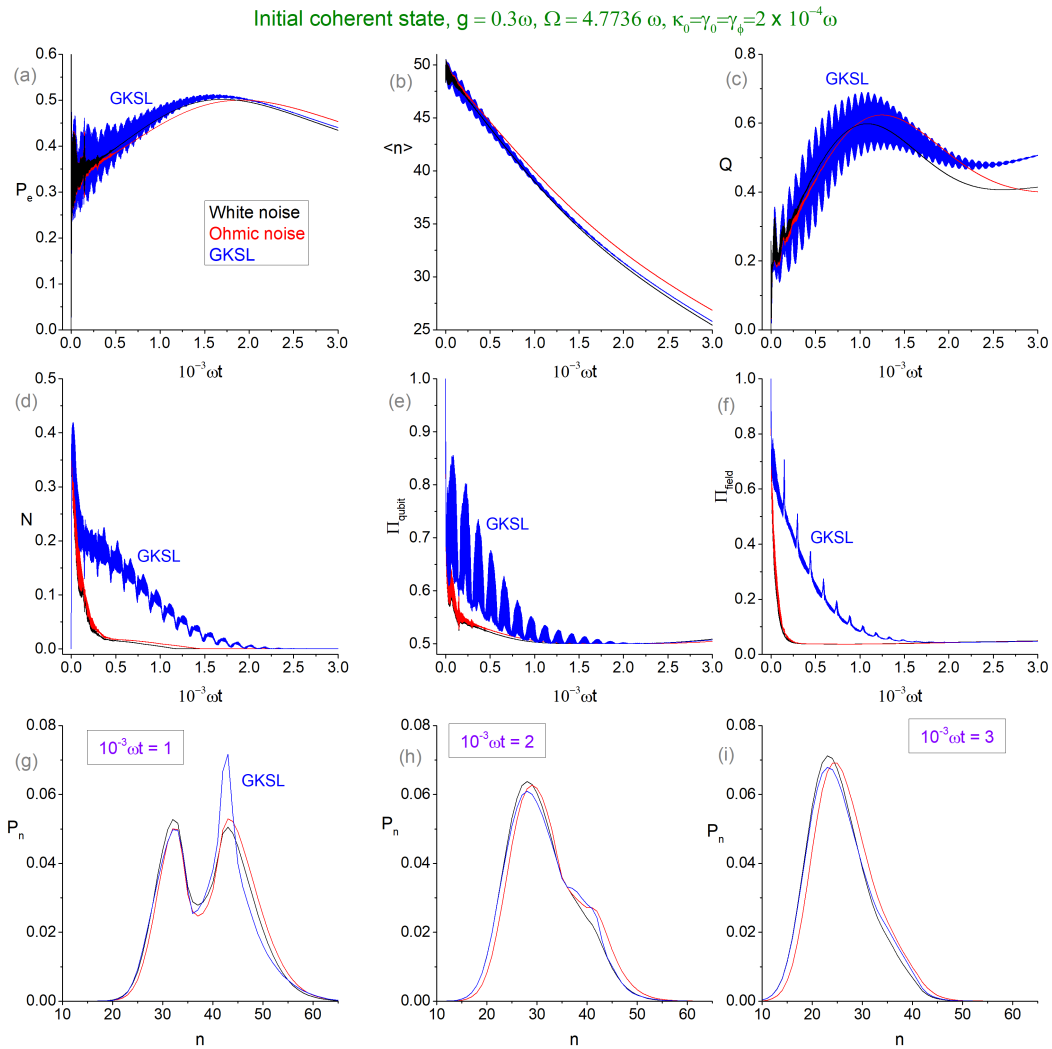

Figure 1.2: Similar to Fig. 1.1 but for parameters $g = 0.3\omega$ and $\Omega = 4.7736\omega$ (in the vicinity of the 5-photon resonance).

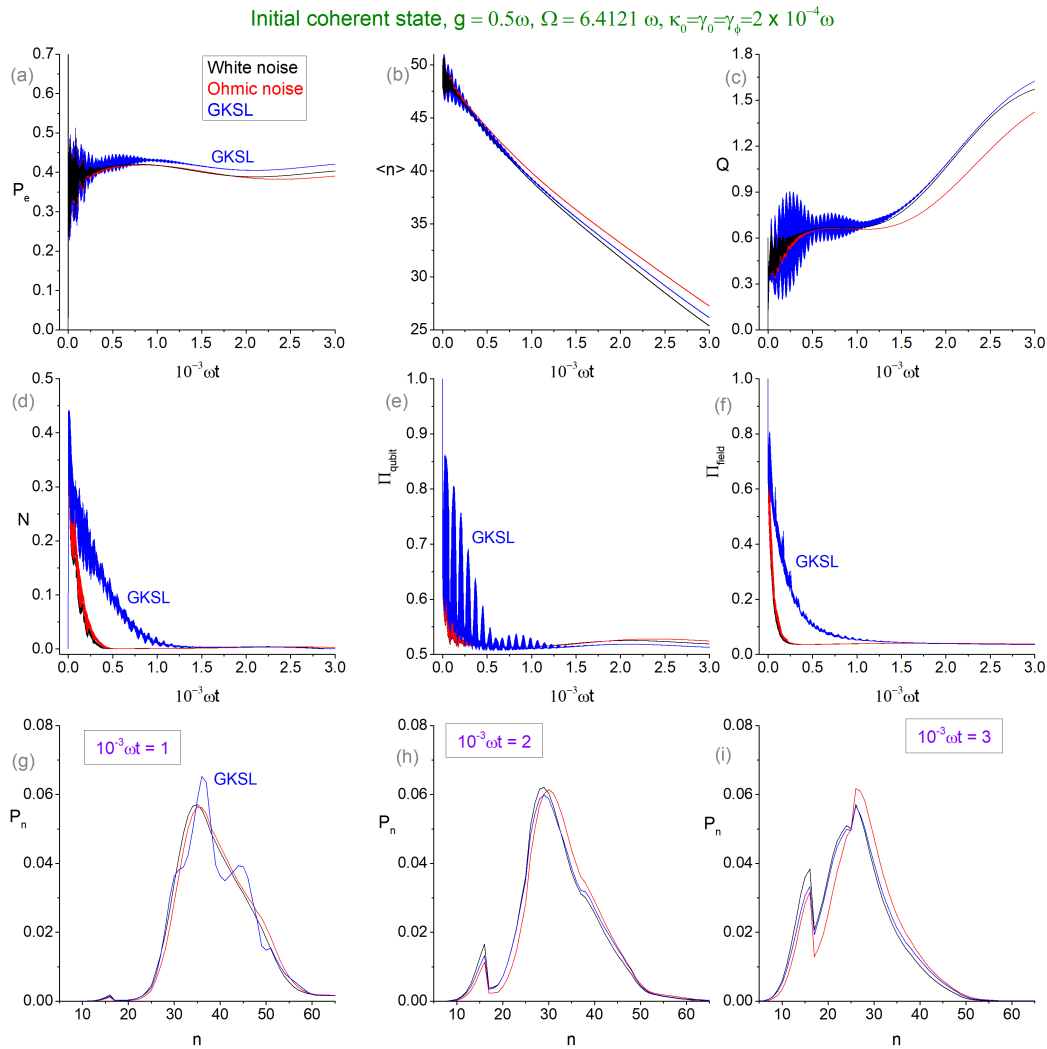

Figure 1.3: Similar to Fig. 1.1 but for parameters $g = 0.5\omega$ and $\Omega = 6.4121\omega$ (in the vicinity of the 7-photon resonance).

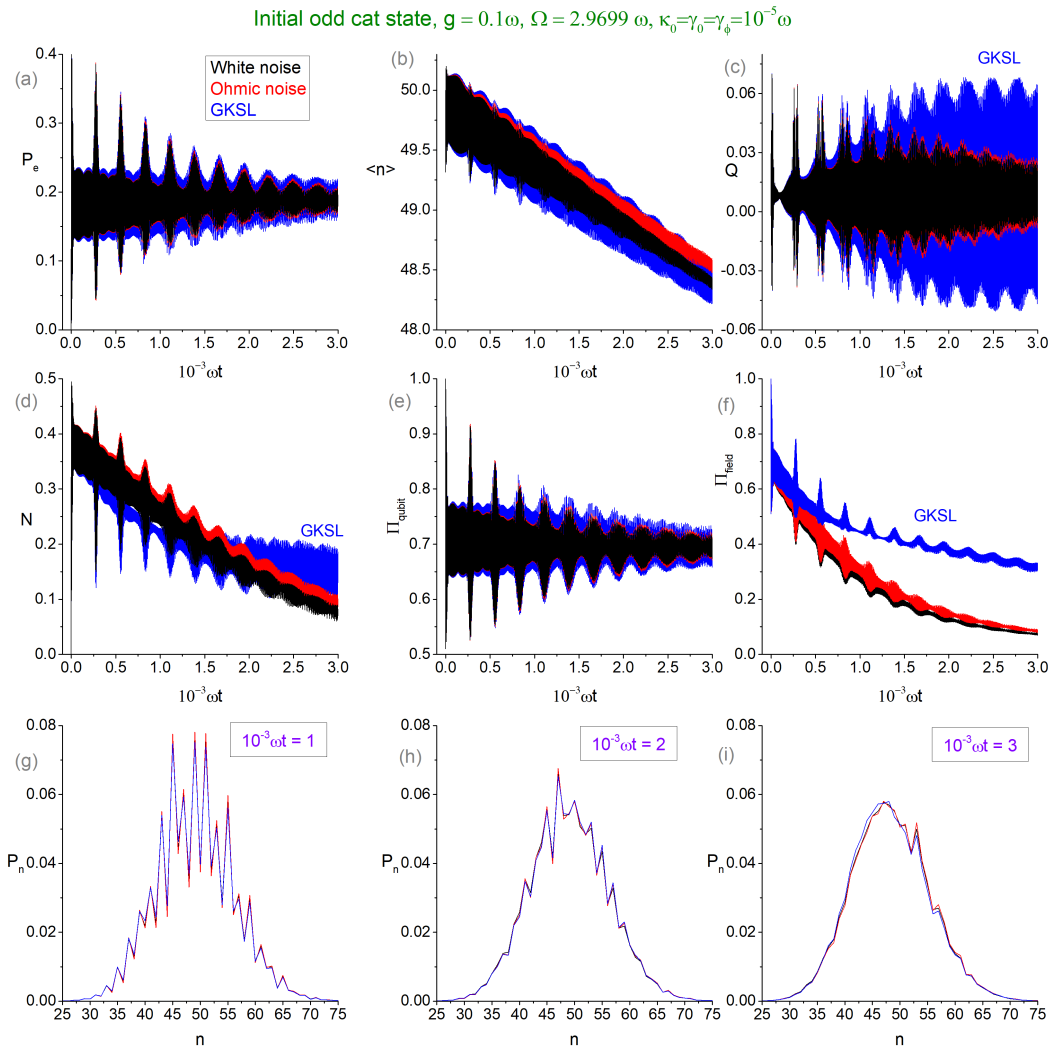

Figure 1.4: Behavior of the quantum Rabi model under dissipation for the initial odd Schrödinger cat state, Eq. (1.66), and parameters $\alpha = 7.071$ (corresponding to $\langle n(0)\rangle = 50$), $g = 0.1\omega$, $\Omega = 2.9699\omega$ and $\kappa_0 = \gamma_0 = \gamma_\phi = 10^{-5}\omega$.

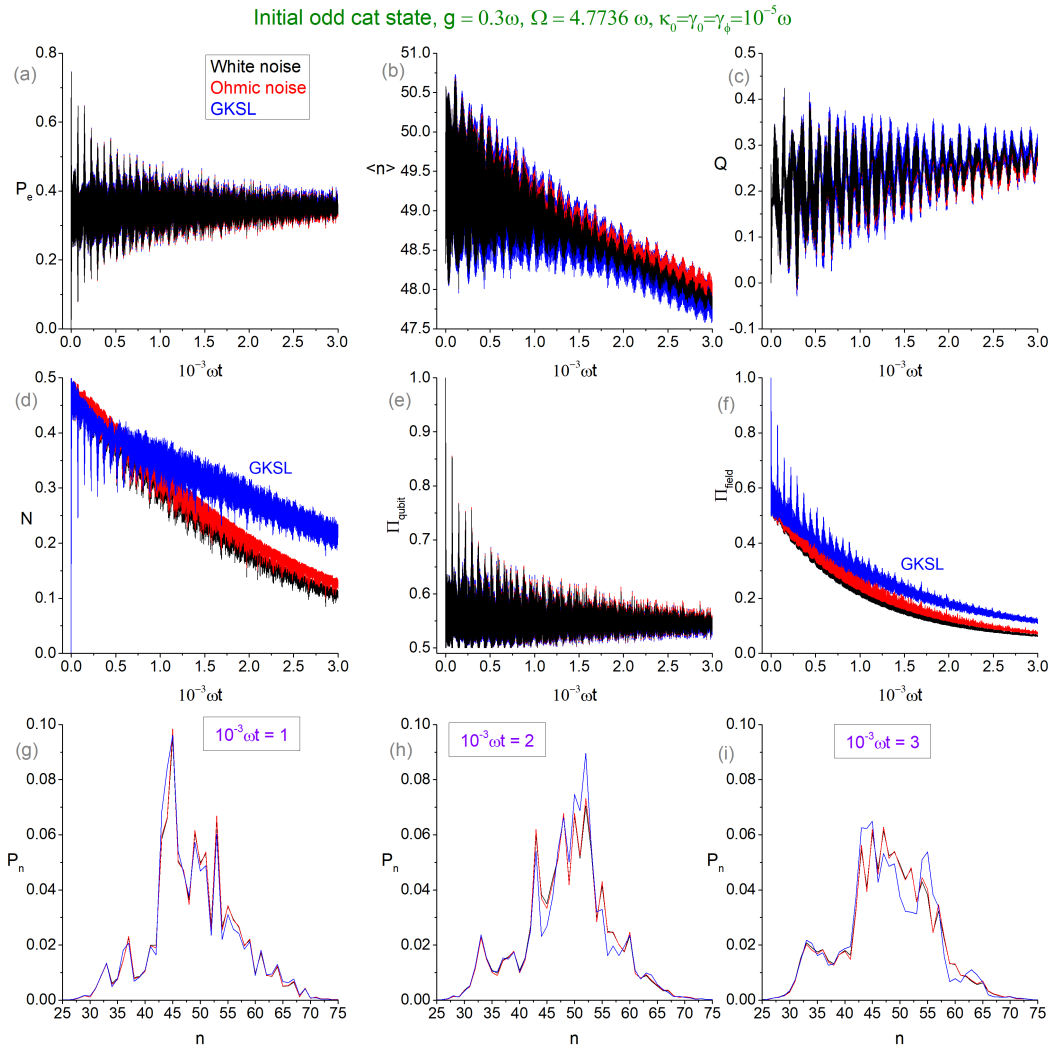

Figure 1.5: Similar to Fig. 1.4 but for parameters $g = 0.3\omega$ and $\Omega = 4.7736\omega$.

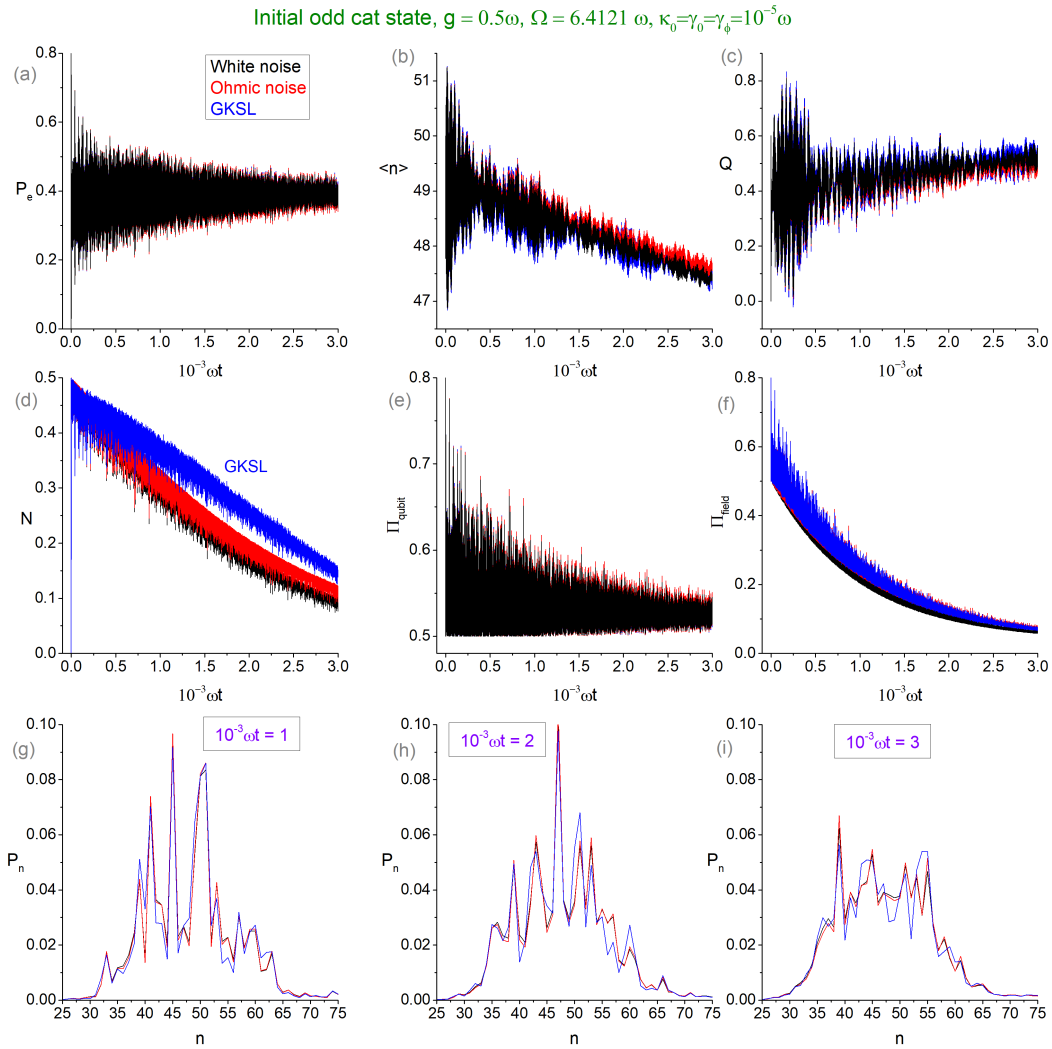

Figure 1.6: Similar to Fig. 1.4 but for parameters $g = 0.5\omega$ and $\Omega = 6.4121\omega$.

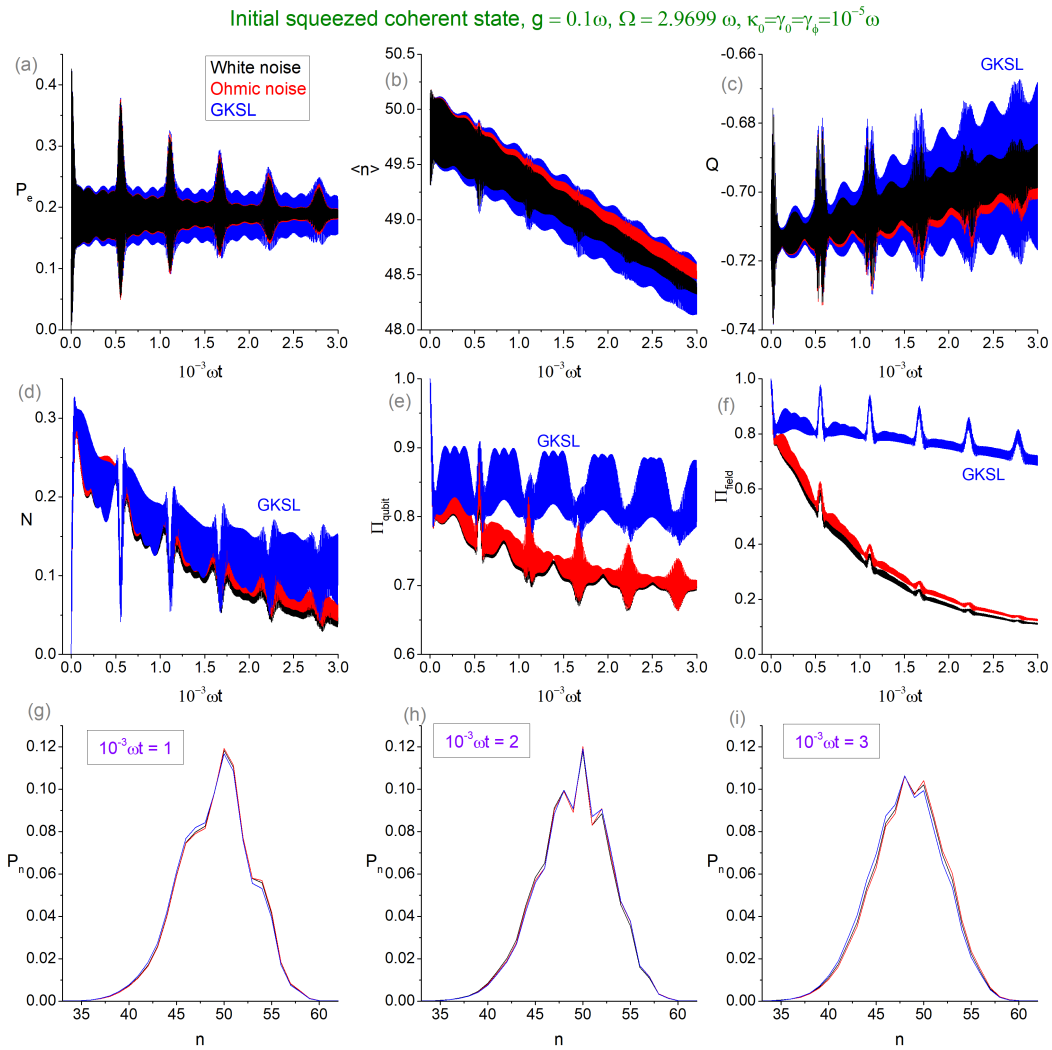

Figure 1.7: Behavior of the quantum Rabi model under dissipation for the initial squeezed coherent state, Eq. (1.69), and parameters $s = 0.7$, $\beta = 14.157$ (corresponding to $\langle n(0)\rangle = 50$), $g = 0.1\omega$, $\Omega = 2.9699\omega$ and $\kappa_0 = \gamma_0 = \gamma_\phi = 10^{-5}\omega$.

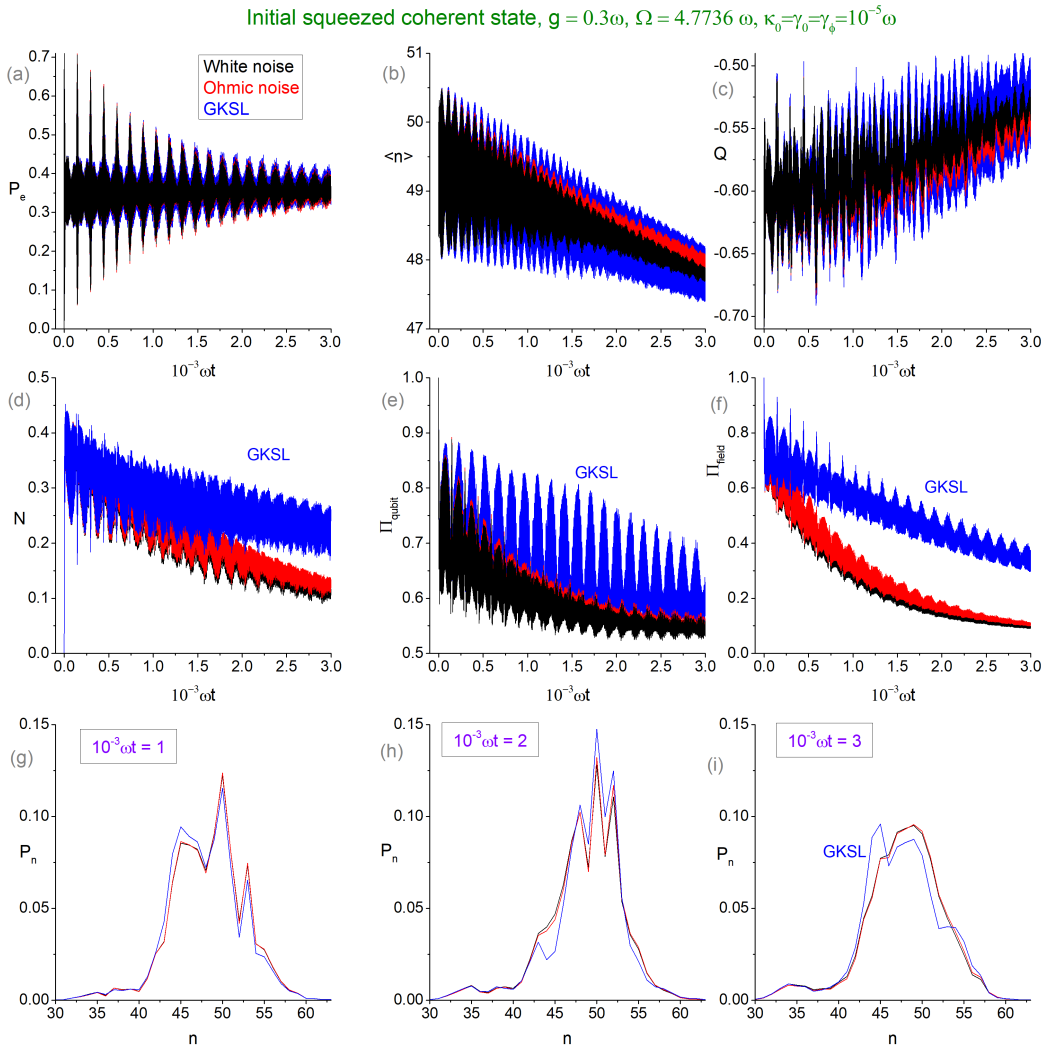

Figure 1.8: Similar to Fig. 1.7 but for parameters $g = 0.3\omega$ and $\Omega = 4.7736\omega$.

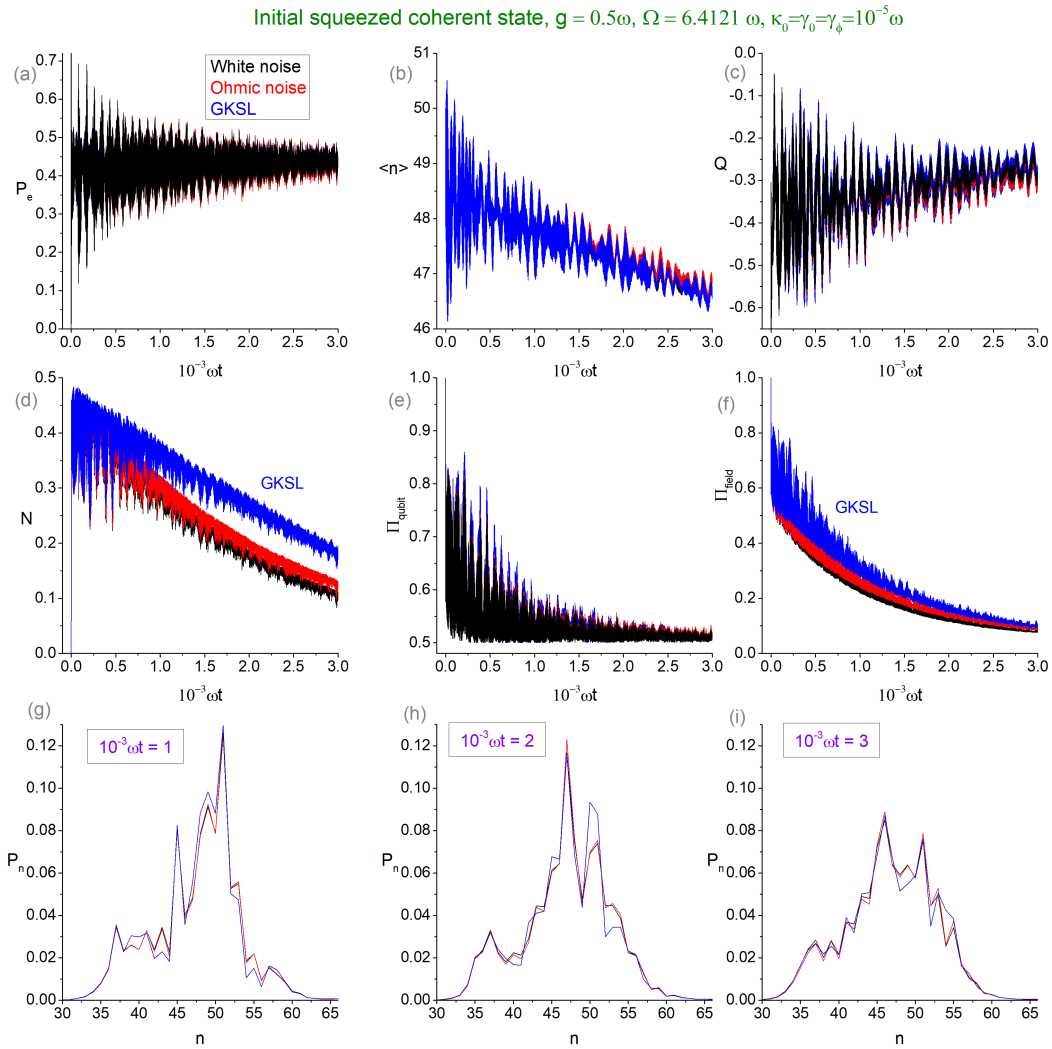

Figure 1.9: Similar to Fig. 1.7 but for parameters $g = 0.5\omega$ and $\Omega = 6.4121\omega$.

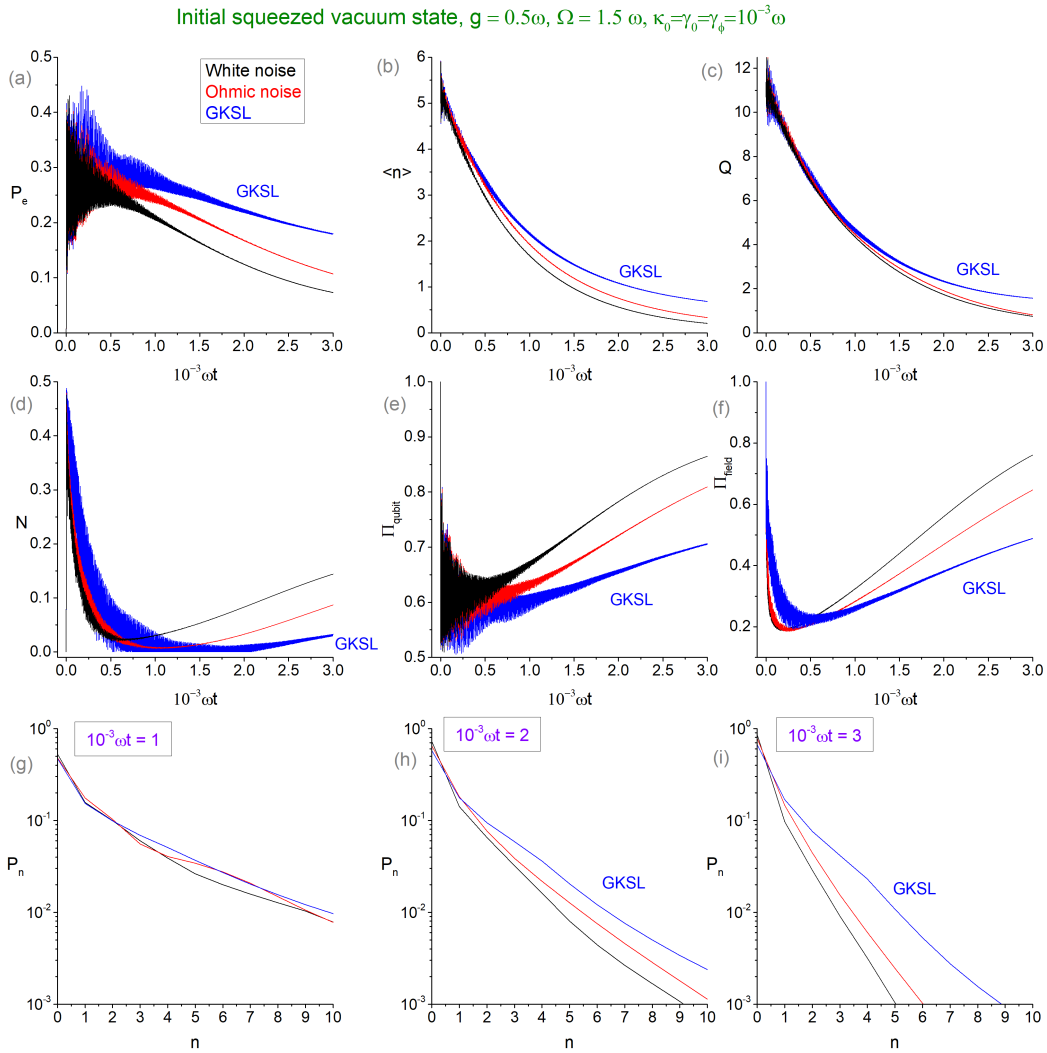

Figure 1.10: Behavior of the quantum Rabi model under dissipation for the initial squeezed vacuum state, Eq. (1.71), and parameters $s = 1.544$ (corresponding to $\langle n(0)\rangle = 5$), $g = 0.5\omega$, $\Omega = 1.5\omega$ (near resonant regime) and $\kappa_0 = \gamma_0 = \gamma_\phi = 10^{-3}\omega$.

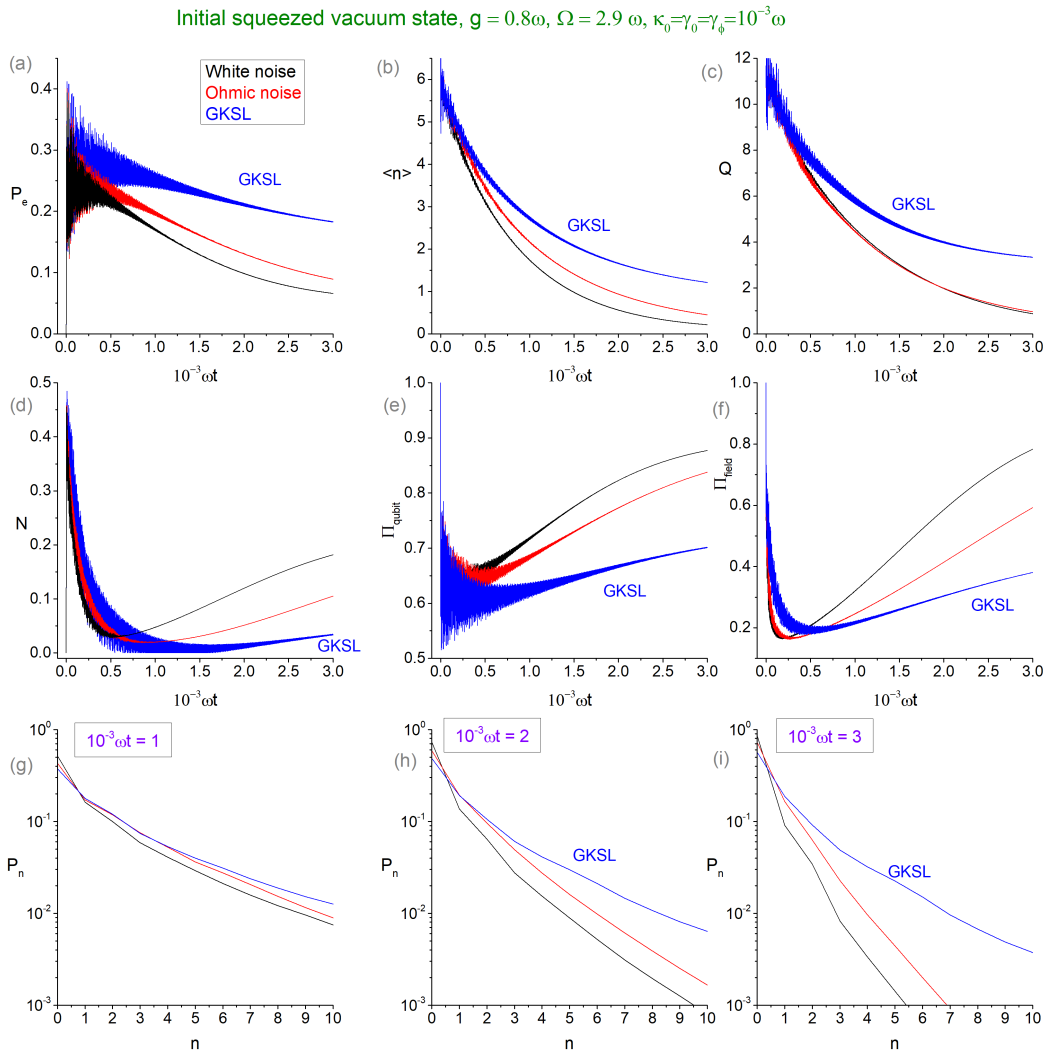

Figure 1.11: Similar to Fig. 1.10 but for parameters $g = 0.8\omega$ and $\Omega = 2.9\omega$.

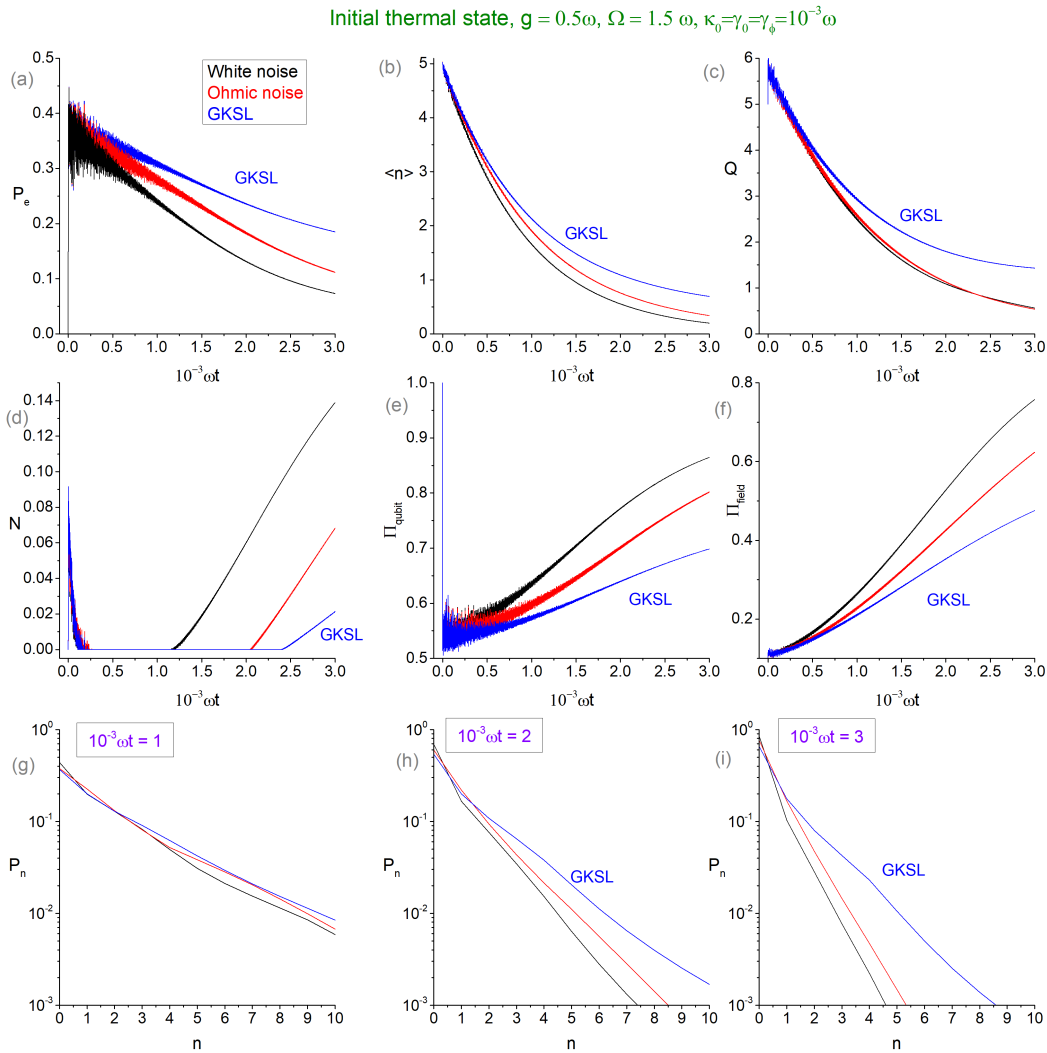

Figure 1.12: Behavior of the quantum Rabi model under dissipation for the initial thermal state, Eq. (1.72), and parameters $\alpha = 5$, $g = 0.5\omega$, $\Omega = 1.5\omega$ and $\kappa_0 = \gamma_0 = \gamma_\phi = 10^{-3}\omega$.

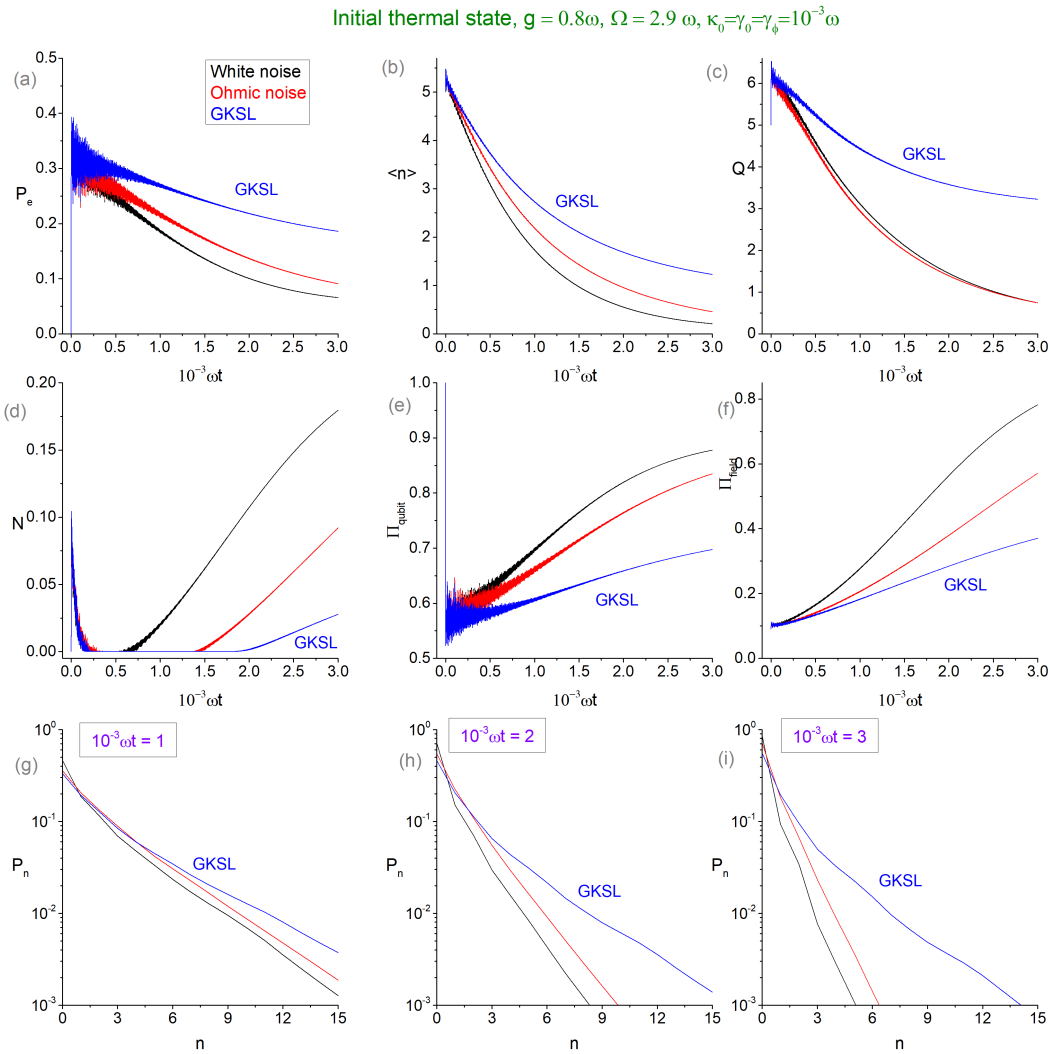

Figure 1.13: Similar to Fig. 1.12 but for parameters $g = 0.8\omega$ and $\Omega = 2.9\omega$.

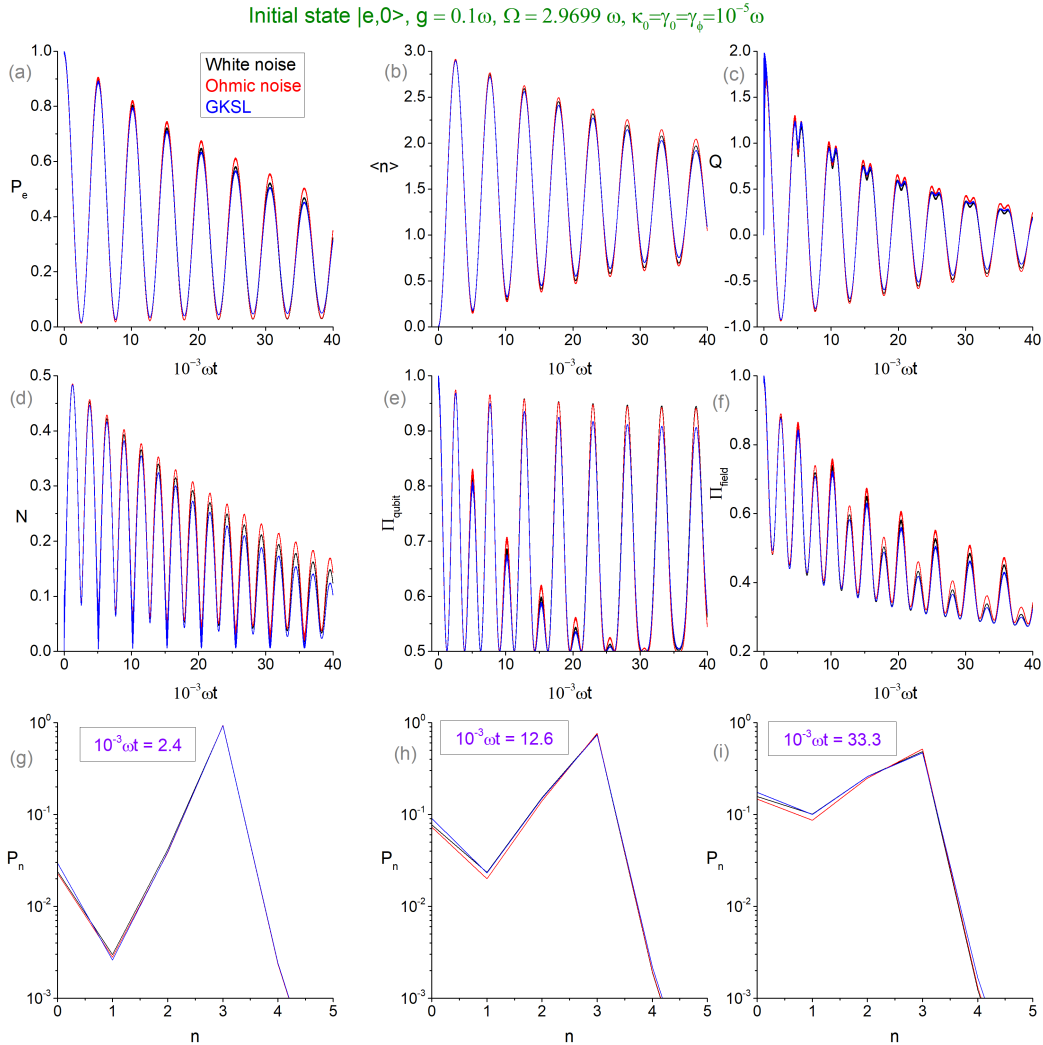

Figure 1.14: Similar to Fig. 1.13 but for the initial state $|e,0\rangle$ and the parameters corresponding to the three-photon light–matter resonance: $g = 0.1\omega$ and $\Omega = 2.9699\omega$.

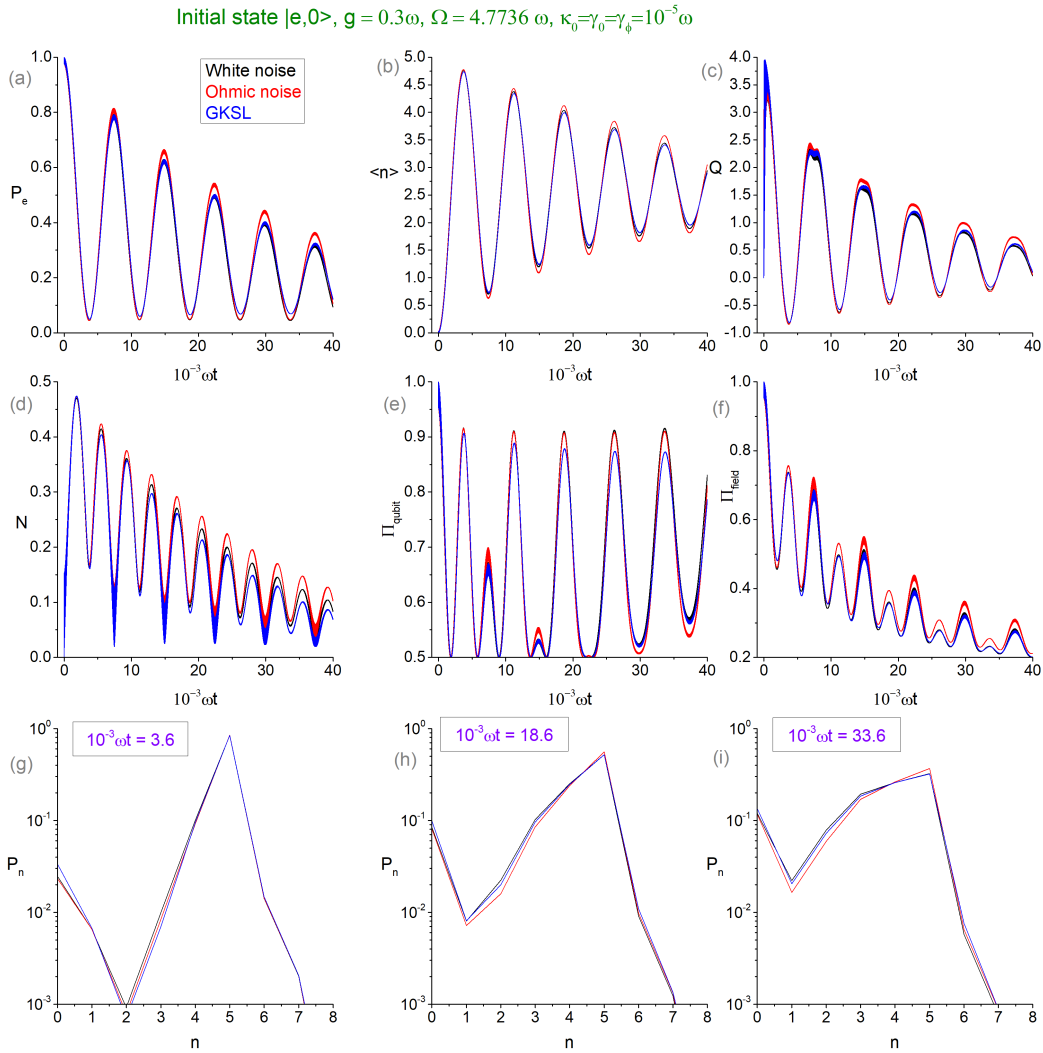

Figure 1.15: Similar to Fig. 1.14, but for the five-photon light–matter resonance: $g = 0.3\omega$ and $\Omega = 4.7736\omega$.

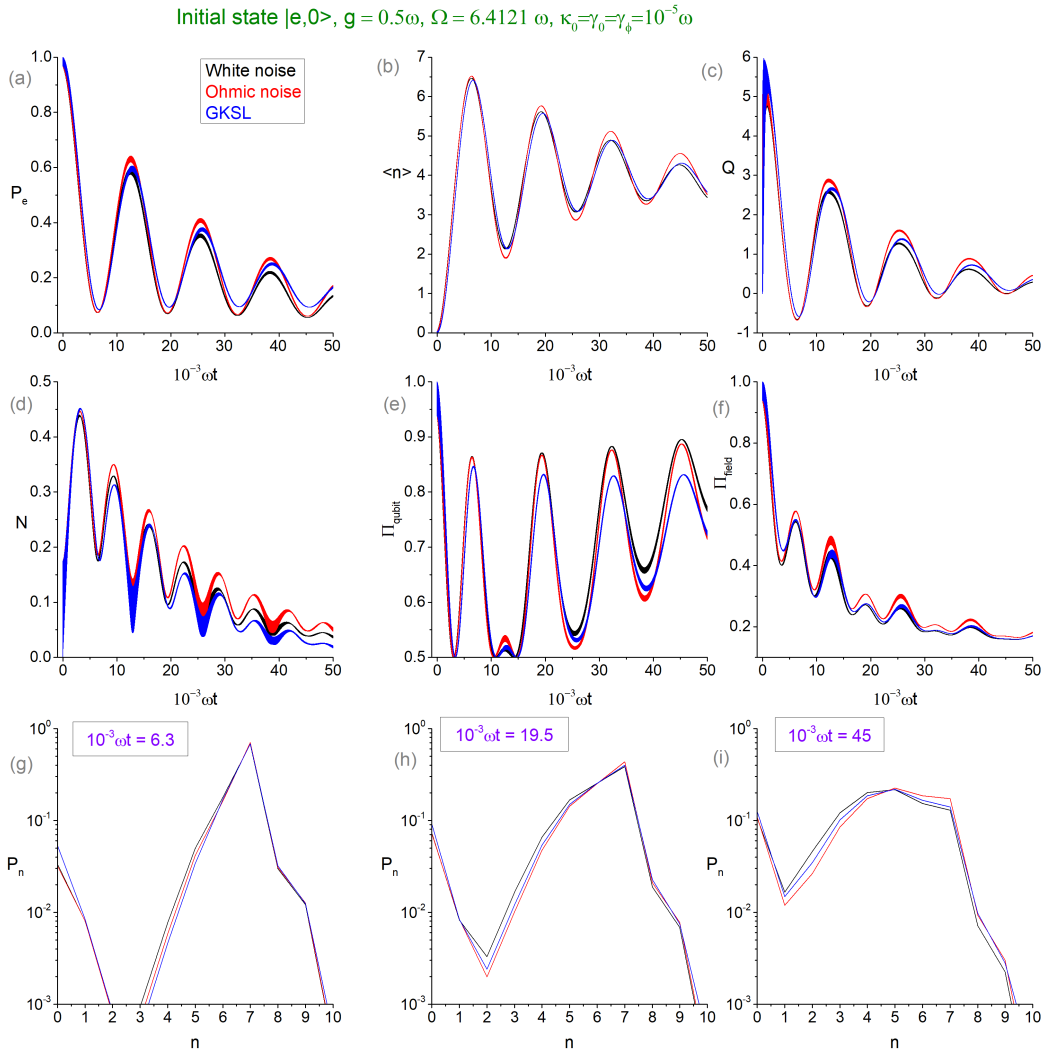

Figure 1.16: Similar to Fig. 1.15, but for the seven-photon light–matter resonance: $g = 0.5\omega$ and $\Omega = 6.4121\omega$.

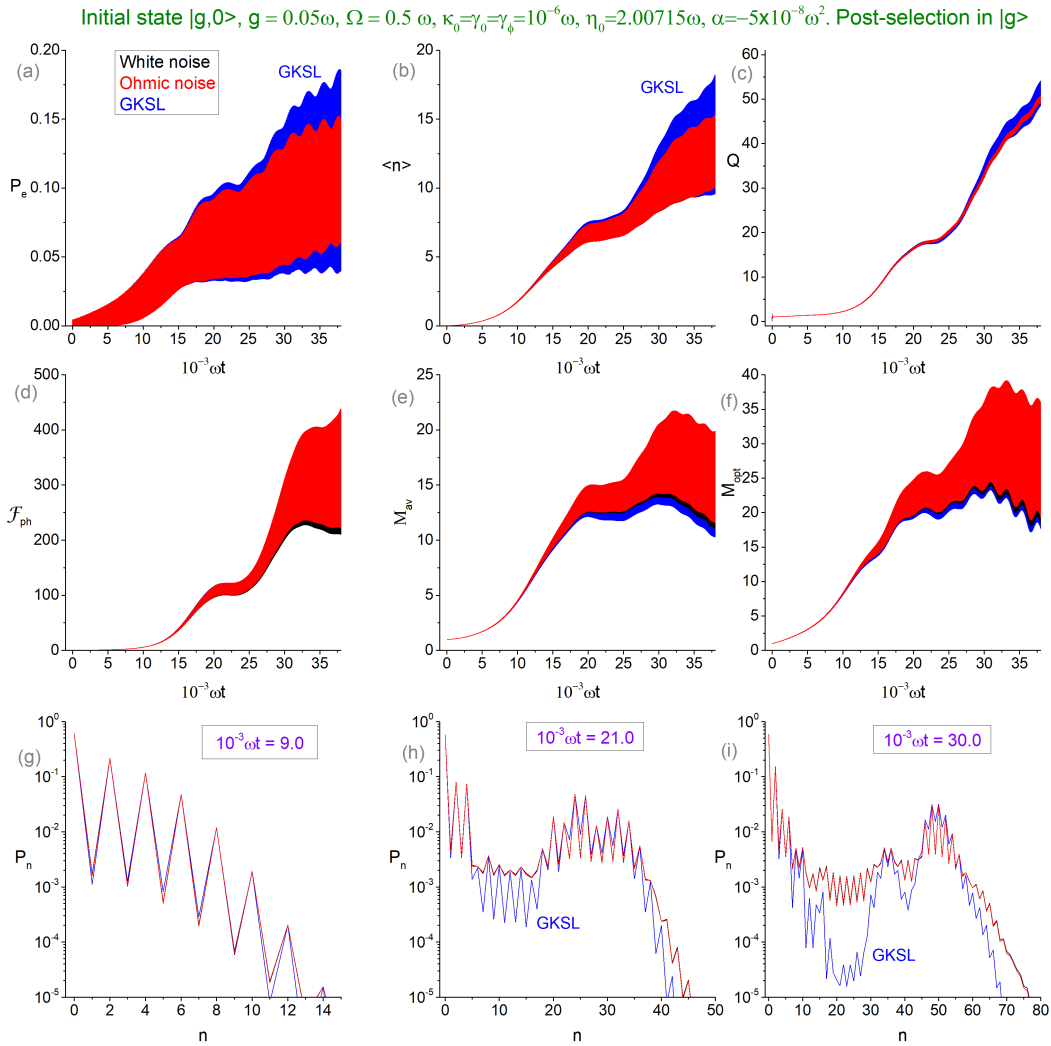

Figure 1.17: Nonstationary Rabi Hamiltonian with time-dependent qubit frequency, Eq. (1.75). a) Qubit excitation probability. b-f) Behavior of the average photon number, Mandel Q-factor, $\mathcal{F}_{ph}$, M_{av} and M_{opt} for the post-selected cavity field state $\rho_{PS}(t)$, which is projected if the qubit is found in the ground state at the time t (with the corresponding probability $P_g = 1 - P_e$). g-i) Photon number probability distribution at some time instants. Parameters: $g = 0.05\nu$, $\Omega_0 = 0.5\omega$, $\varepsilon_\Omega = 0.08$, $\gamma_0 = \gamma_\phi = \kappa_0 = 10^{-6}\omega$, $\eta_0 = 2.00715\omega$ and $\alpha = -5 \times 10^{-8}\omega^2$. The nonzero probabilities of odd photon numbers are due to the dissipation.

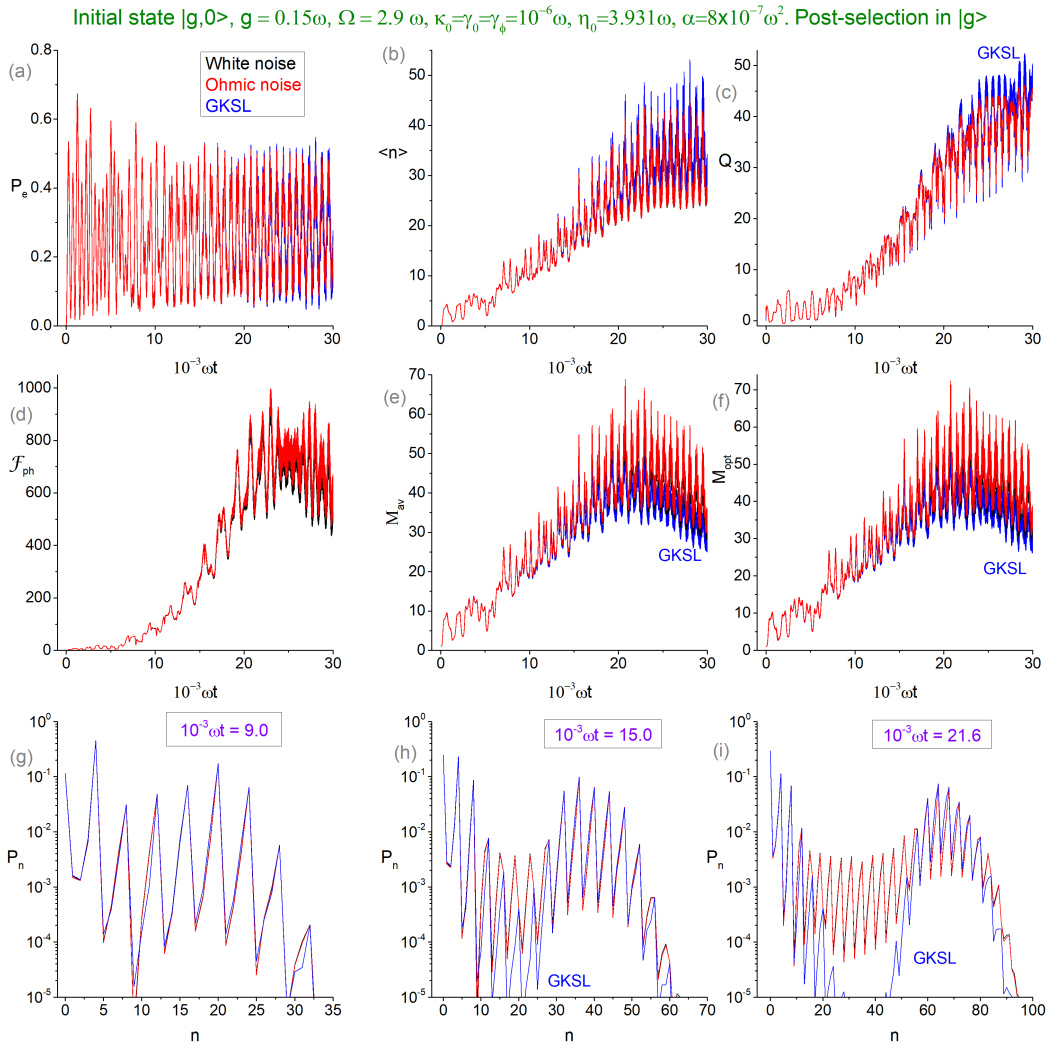

Figure 1.18: Similar to Fig. 1.17 but for parameters $g = 0.15\omega$, $\Omega = 2.9\omega$, $\eta_0 = 3.931\omega$ and $\alpha = 8 \times 10^{-7}\omega^2$. This modulation frequency induces 4-photon transitions between the system dressed states, as attested by the panels (g)-(i).